ABSTRACT

NEHAL N. DESAI. Investigations in Gas-Solid Multiphase Flows. (Under the direction of Professor Kevin M. Lyons.)

Gas-solid multiphase flows are used extensively in both science and industry. Understanding these flows is great commercial and academic interest. One tool use to further our understanding of solid-gas flows is theoretical and computer modeling. One of the least understood areas of multiphase flows is the momentum transfer or coupling of the phases. Depending on the nature of the flow, such momentum transfer can have substantial effect on the flow. In this thesis, we investigate two novel and interesting aspects of momentum exchange in gas-solid multiphase flows. Until recently, Euler-Lagrangian techniques were only applied to dilute solid-gas flows, because of the computational expense required to calculate the particle-particle interactions. The first investigation in this thesis deals with extending the Euler-Lagrangian to dense solid-gas flows and the modifications required to make this technique a viable alternative to continuum techniques. The results of the various simulation and comparisons are presented and in general are in very good agreement with experimental data; capturing unique and previous unreported experimental features. In the second investigation, we apply inverse parameter estimation to the problem of determining the coefficients of an generalized Ergun type momentum exchange. The results of the investigation indicate that for flows under consideration, the momentum exchange term has small influence on the flow. This would also explain many of the results reported in the literature which use simplistic or physically unrealistic momentum exchange.

Investigations in Gas-Solid Multiphase Flows

by

Nehal Desai

A thesis submitted to the Graduate Faculty of
North Carolina State University
in partial fulfillment of the
requirements for the Degree of
Doctor of Philosophy

Mechanical Engineering

Raleigh

2003

APPROVED BY:

Chair of Advisory Committee

BIOGRAPHY

Nehal Desai was born in Charlotte, North Carolina. He attended North Carolina State University... and finally graduated. Nehal is now happy.

Contents

List of Figures

List of Tables

Chapter 1

Introduction

1.1 Introduction

Multiphase flows are encountered in many important engineering and environmental systems. Because of there commercial importance understanding and improving multiphase processes has become an active area of research. To improve multiphase systems requires among other things a better understanding of the multiphase flow physics. One of the most important tools to improve our understanding of multiphase flow is computer modeling. With recent advances in computer hardware and software, the ability to model complicated phenomena like multiphase flow has never been greater. However, multiphase flows are complex and correctly understanding the assumptions and limitation of the computer (and theoretical) models is vital to process optimization. This thesis re-examines many of the basic assumptions used in the computational and theoretical modeling of multiphase flow and aims to find alternate strategies and approaches that permits the modeling of these flow more effectively.

Multiphase flows are generally divided into four categories: gas-liquid, gas-solid, solid-liquid and three phase flows. The table below shows these categories in more detail. This study focuses on the second type of multiphase flow; gas-solid or dispersed flows. Gas-solid flows are perhaps the most common type of multiphase systems and are used in a number of important chemical processes including: the fluidized catalytic cracker, pneumatic transport of material, and pollution control systems. This introduction is based on a number of excellent reviews of gas-solid transport.

gas-liquid flows	Bubbly Flows Separated Flows Gas-Droplet
gas-solid flows	Gas-Solid flows Pneumatic flows Fluidized Beds
liquid-solid flows	Slurry Flows Hydrotransport Sediment Transport
three-phase flow	Bubbles in slurry flow Droplet/particles in gaseous flows

Table 1.1: Examples and categories of multiphase flow

Loth [41] is a comprehensive introduction to the numerical approaches used to model gas-solid flows. Crowe, Tsuji and Sommerfeld [17] is excellent introductory book to gas-solid flows. Many of the topics discussed in this introduction are given a fuller treatment in this book. Enwald, Pierano and Almstedt [28] discuss the application of Eulerian techniques to the fluidizing systems and give a complete derivation of two-fluid multiphase equation.

1.2 Gas-Solid Phase Overview

Gas-solid multiphase flows appear in a number of important industrial and environmental applications including: fluidized beds, pollution dispersion and pneumatic transport. Gas-solid multiphase flows are the concurrent flow of solid particles in a gas stream. Depending on how the solid particles interact with one another and the gas phase, gas-solid flows can be subdivided into broad two categories: dilute

and dense gas flows. Though descriptive, the terms dilute and dense are ambiguous and give little insight into the flow physics or modeling approaches. In the next few sections we will

- Review criteria to determine the type of flow (dilute or dense).
- Review the impact of this categorization on modeling approaches.

1.2.1 Criteria for gas-solid flows

As stated previously, the key factors in determining whether a flow is dilute or dense is the type and magnitude of the interactions between phases. These interactions can be of two types: interaction between the constitutive elements of the solid phases (the interparticle interaction) and the interaction between the solid and fluid phases. The interaction between particles is further subdivided into: collisional interactions and hydrodynamic interactions (lubrication interactions). By comparing the various gas, solid, and collisional timescales, criteria have been established to determine the density (or relative density) of the multiphase flow. Loth [41] gives a number of interesting criteria for dilute flows. The most widely used measure of the gas-solid flow density is the mass loading, which is the ratio of the solid phase mass flux to the fluid phase mass flux.

$$Z = \frac{\bar{\rho}_p v_p}{\bar{\rho}_f v_f} \tag{1.1}$$

Here $\bar{\rho_p} = n_p m_p$ and $\bar{\rho_f} = (1 - n_P V C_p)\rho_f$. Using the well know relationship between density,mass and volume and assuming that particles are spheres and can never exceed the total volume ($n_p V_p \leq 1$). We can get the relationship.

$$Z = \left[\frac{n_p V_p}{1 - (n_p V_p)}\right]\left[\frac{\rho_p}{\rho_f}\right]\left[\frac{v_p}{v_f}\right] \tag{1.2}$$

Inaddition to establishing criteria for dilute and dense phase flows, timescale analysis is useful in the determining the interactions of a single particle with the gas phase. The degree to which a particle maybe in kinetic equilibrium with the surrounding gas is given by the ratio of the particle timescale to the fluid timescale.

$$St = \frac{\tau_p}{\tau_f} \tag{1.3}$$

The Stokes number dictates how readily a particle follows the flow. For laminar flows this relationship is straightforward.

$$St = \frac{n_p \pi \rho_p d_p |v_f - v_p|}{18\mu} \tag{1.4}$$

The Stokes number for turbulent flow is more problematic, because of the many timescales associated with turbulence and turbulent flow. In the turbulent flow case, the Stokes number represents the relative importance of turbulence on the particle motion [20]. In both the laminar and turbulent cases a Stokes number less than

unity means that a particle acts as diffusive tracer and can quickly respond to fluctuates in the flows. For Stokes numbers greater than unity particles do not respond quickly to changes in the flow. Taken together, the mass loading and Stokes numbers portend one of the central issues/problems of gas-solid multiphase flows – phase coupling. Depending on how the phases interact, phase maybe coupled in three ways: mass coupled, momentum coupled and energy coupled. If the gas and solid particle exchange momentum they are said to be momentum coupled. Momentum coupling provides the vital link between mass loading, the Stokes number and the modeling approaches of the next section. In general

$$\Pi_{mom} = \frac{Z}{(1 + St)} \tag{1.5}$$

which implies that momentum transfer (Π_{mom}) increases with increased mass loading (Z). This is consistent with our understanding of the types of interactions (collisions) that can dominate dense phase flows. Conversely in dilute flows (small Z) there is little exchange of momentum between the particles or the particle and the fluids. Dispersed flows that exchange momentum between the phases are said to be 'two-way' coupled.

1.2.2 Modeling approaches

Until recently, the type of computer model used to explore gas-solid flows depended on the "density of flow" as defined by the mass loading or other flow metrics [41]. Dense gas-solid flows like those in a fluidized catalytic cracker, were modeled by extending fluid continuum models,which assume that the primary characteristics of the multiphase system (void fraction, particle velocity, etc) could be described by continuum equations in a fixed or Eulerian reference frame. Dilute flows (low Z and low Π_{mom}) were modeled using Lagrangian models,which treat the solid phase as discrete particles that are individually tracked through the fluid phase. These methods are described in more detail below.

Eulerian Models

Ishii [37] divides the Eulerian approach into two types: diffusion and two fluid. Diffusional models (or the local homogeneous formulation) represent the gas-solid mixture as a whole with one continuity equation, one momentum (in each coordinate directions) equation , one energy equation and one diffusion equation. Diffusion models assume that the particle and the fluid are in local kinetic and thermal equation. In the laminar flow case, the diffusion model reduces to a variable density single phase flow formulation. The most commonly used Eulerian model is the two-fluid model, which treat the gas and solid as two separate inter-mixed continua. Two-fluid models have continuity, momentum and energy equations for each phase and are closed using

empirical or semi-empirical constitutive and transfer equations. In general two-fluid models seek to apply volume averaging [28] [62] [22] techniques to the instantaneous equations of motions for each phase. The result is a Navier-Stokes-like set of equations for each phase with additional closure equations. Implicit in the averaging process is the understanding that the interphase expressions are based on a point-volume description of the particle. Closure equations are of three types: constitutive, transfer and topological.

- Constitutive equations specify how the physical properties of the phases interact with one another other, but do not describe the mass, momentum or energy transfer between them. Examples of the physical parameters that can/are predicted with the constitutive equation include: the viscous stress, particulate phase bulk and dynamic viscosity and particle pressure. Many constitutive equations are based on empirical models of particle properties and the void fraction. The most recent models use the kinetic theory of granular flows to develop many of the constitutive relationships [31].

- Transfer equations describe mass, momentum and energy exchange between the phases. The momentum transfer equations often appear in the multiphase Navier-Stokes equations as source terms. Because of the complicated nature of the solid-solid and solid-gas interaction these equations are often empirical or semi-empirical correlations. The nature and effect of these drag function on dispersed flows is the primary focus of chapters 2 and 3.

- Topological equations are used to describe the spatial distribution of a flow variable.

The Eulerian approaches have a number of advantages over the Lagrangian approach. The primary one being less computational expense (for approximately the same type of problem). In general Lagrangian methods require that each particle and its associated characteristics be stored during the calculations. It is easy to see that for even moderately dense flows the associated memory and computational requirements may be quite large. Because Eulerian methods are grid-based, memory and the computational requirements do not change radically with the introduction of additional particles. However, a number of problems exist with two-fluid models including: the type and nature of the boundary conditions for wall-bound flows, where the tangential particle velocity will not be zero as it is for the fluid phase; polydisperion of particle size and the sometimes dubious nature of the gas-solid and solid-solid momentum exchange terms. This last problem is addressed in more detail below in this thesis.

Lagrangian methods

In Lagrangian methods the individual solid particles are tracked through the fluid phase. Lagrangian methods can be formulated in two ways depending on the type of flow physics being studied. The most commonly used Lagrangian formulation is the point mass representation of a particle. In this representation the particle is much smaller than the grid spacing on which the gas velocity is calculated and does not

influence the gas domain or its discretization. The point mass techniques are used to model large numbers of particles without regard to the specifics of the gas-solid fluid mechanics (e.g. boundary layer effects). In the point mass representation the trajectory of the particles through the gas phase is determined by integration of the particle equation of motion (PEM) which is based on the forces that are *assumed* to act on the particle. If the particle diameter is larger than the grid spacing (we have a very fine grid), the resolved volume representation is used. Resolved volume approaches avoid the modeling assumptions present in the point mass representation (e.g. PEM) by discretizing the three dimensional particle flowfield. Thus producing a more detailed understanding of the gas flow around particles. However, this results in greater computational expense per particle, which makes the resolved volume method unsuitable for engineering applications where many particles must be modeled. The point mass and resolved volume representation can be thought as complimentary techniques. Often, resolved volume calculations are used to examine the assumptions of point mass techniques. According to Loth [41] strict application of the point mass method requires the particle diameter to be smaller than the characteristic microscale eddy length, which for turbulent flow is the Komologrov scale. Most turbulent flows of interest to engineers do no meet this criteria (e.g. $d_p \leq \lambda_k$). Thus, the results of these calculations must be interpreted with caution. Even, when this criteria is loosened such that the point mass method only requires resolution of turbulent fluctuation down to the scale where the instantaneous velocity is than the

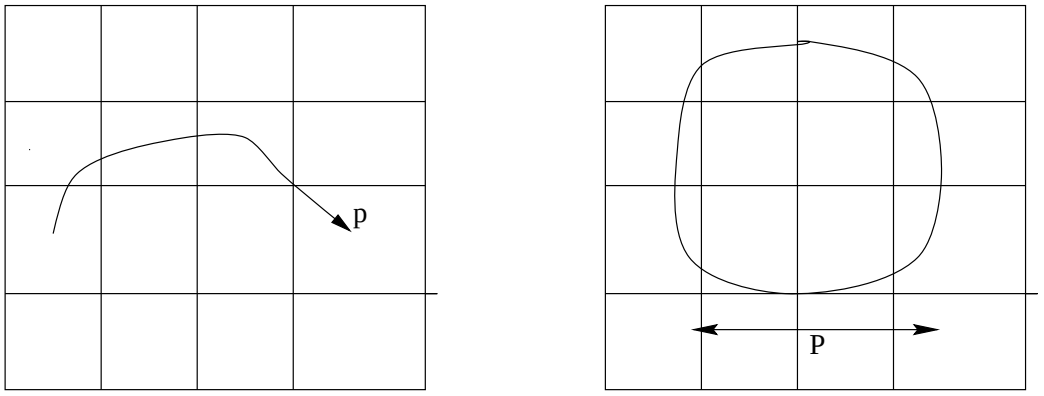

Figure 1.1: a. Point mass and b. Resolved volume

terminal velocity of a particle in a quiescent fluid, the Reynolds Averaged Navier Stokes (RANS) method is unsatisfactory as there are no spatially resolved turbulent structure in these approaches. When RANS methods are used to calculate the gas phase velocities, a modification of the point mass method is used. The "cell-averaged" point mass models the spatial and temporal turbulence within the grid cell in order to predict their influence on the particle momentum equation. In addition, the influence of the instantaneous velocity fluctuations at the particle must be modeled. How turbulent flows effect particle motion is described in excruciatingly detail by a number of authors.

1.3 Applications

Gas-solid phase flows have a vast number of applications in technological systems. Typical gas-solid flows include: fluidized bed reactors, particle generation, solid

transports and separations processes. Like many current research areas, the study of gas-solid flows emerged from a practical need to understand commercial processes. Perhaps because of this genesis much of the research in gas-solid flows is in framed in terms of benchmark applications like the fluidized catalytic crackers and pneumatic transport. In addition to their commercial value, these systems have interesting hydrodynamics properties, which often are the same properties that make/made it an commercially important. In the next section, the hydrodynamics of multiphase flows is examined in the context of these applications. The purpose of examining these applications in detail is to 1). Provide motivation to the rest of the study 2). Provide a reference framework for later discussions 3). Provide an introduction to the wide range of hydrodynamic phenomena produced by multiphase flows.

1.3.1 The Fluidized Catalytic Cracker

Perhaps the most commercially important of all multiphase processes is the fluidized catalytic cracker (FCC). The FCC is used to produce gasoline and naphthalene from virgin gas oil (i.e. a refinery). At the heart of the FCC is the fluidized bed. A fluidized bed is a large open vessel containing granular material (e.g. sand) supported by a plate spanning the bottom of the vessel (3.3). Generally, the plate is porous and gas is forced upward through it. As the gas flows through the bed, the solid and gas phases interact. Initially, the solids in the vessel are stationary however, as the gas velocity is increased further, the solids start to move or "fluidize". It is this intense

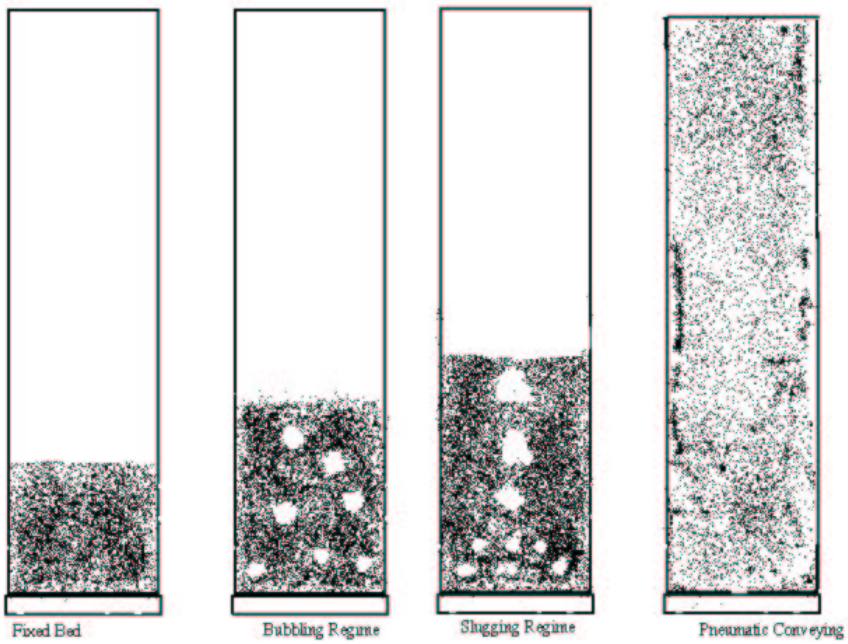

Figure 1.2: Transition points in a fluidized bed

solid-gas interaction that makes the fluidized bed ideal for solids mixing and heat transfer. The large air-solid interface make fluidized beds ideal for catalytic reactions like those necessary to "crack" hydrocarbons. As a fluidized bed transitions, the gas-solid interaction produces a number of interesting phenomena. Perhaps the most striking (and most studied) hydrodynamics phenomena of the fluidized bed is "bubbling". When a fluidized bed "bubbles" gas-filled area appear which rise in the solid phase; much like the formation of gas bubbles in a liquid. A good understanding of bubbling is necessary to understand such phenomena as solids mixing, reaction conversion, heat and mass transfer, erosion and particle entrainment. Bubble formation

has proven a difficult challenge for the experimentalist as well as the theorist. Segregation is the migration of small or light particles upward while the heavy particle travel downward in a bubbling fluidized bed.

Fluidized beds are prime examples of a dense phase flow, in which particle-particle collisions are the primary mechanism for interphase mass transport. Fluidized beds are one of the primary applications used to benchmark two-fluid Eulerian models, although a few researchers have attempted to use Lagrangian methods (or one its variations) to model fluidized bed system. Perhaps the hardest hydrodynamics feature of the fluidized bed for most current model to capture is bubbling. The figures below show the results of a typical fluidized bed bubbling calculation. The air enters the bed through a single opening (1.37 cm OD) at the centerline (below the obstacle) at a velocity of 5.77 m/s. The bed material is composed of 880μ m particles with a density of 2.42 g/cm^3. The bed is 20 cm from the centerline to the wall. The simulation time was 1.5 seconds. The figures below show the rise of a single bubble in a fluidized bed with an immersed obstacle. The figures show the time evolution of solids volume fraction as bubble rises through the FCC. The darker regions have a higher solids concentration. Figure 1.3.1 shows the time-averaged air fractions (ϵ_f) at 3 locations in the bed.

The example above is primarily for illustrative purpose. However, it is easy to see that the current two-fluid Eulerian models can capture some of the gross properties of dense gas solid flows, however to capture the finer features of the flow requires a

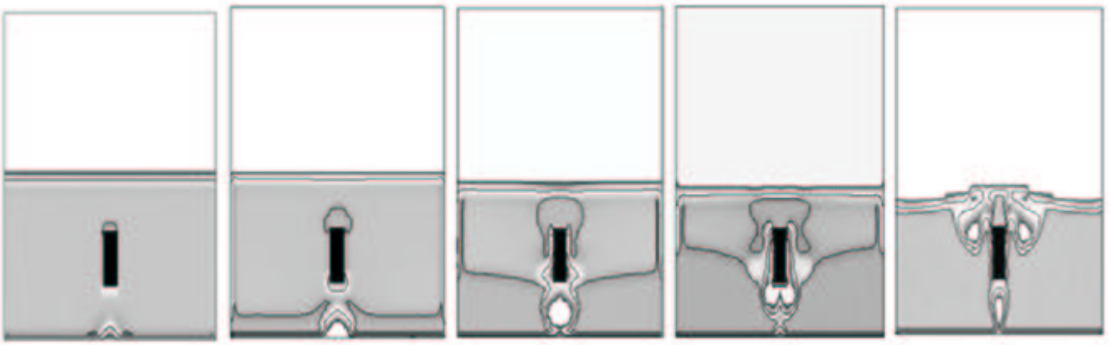

Figure 1.3: Evolution a bubble in a fluidized bed with obstacle. Increasing time from left to right.

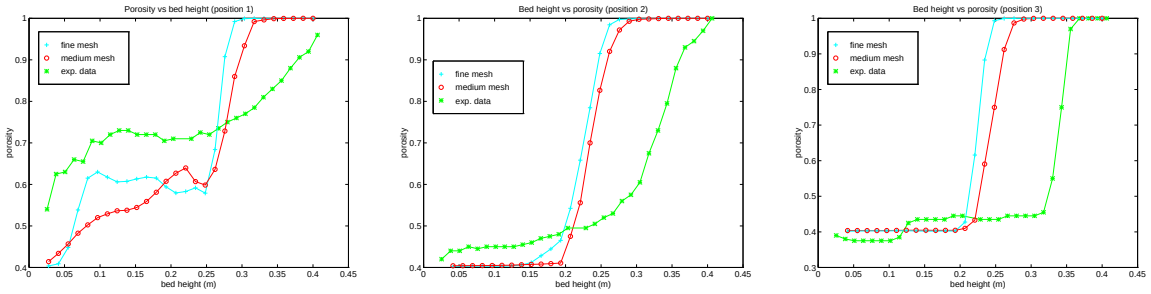

Figure 1.4: Time Averaged solid void fraction at 3 locations. (a). Position 1 is 3 cm from the centerline (b). Position 2 is 10 cm from the centerline (c) Position is 17 cm from the centerline

more sophisticated understanding of the physics involved.

1.3.2 Pneumatic Transport

A second "benchmark" application is pneumatic transport or the transport of material by air. Because of its simple geometry, pneumatic transport has become a favorite test application for test experimental and computational models for multi-

phase flows. A typical pneumatic particles in pipe (PIP) experiment is shown below. A number of experiments have been done which study the flow of air and particle in pipe. Tsuji [71] [70] examined both the horizontal and vertical piping systems. The experiments for vertical pipe reveal a number of interesting phenomena including a skewing of the maximum gas velocity. For single phase mildly turbulent pipe flow, the maximum velocity is at the centerline of the pipe, however for gas-solid flow at moderate mass loading (ml=2.1-3.1), the maximum velocity shifts away from center. As the loading increases the gas phase velocity shifts further away from the center. Durst and Lee also conducted a series of experiments in which they measured the particle and gas-phase velocity of several different size particles and different mass loading.

1.4 Purpose and motivation for this study

The introduction above gives a very brief description to a complex and complicated physical phenomena. The purpose of this study is to examine two potentially interesting extension to multiphase theory.

1.4.1 Application of inverse theory to two-fluid multiphase flows

The first idea explored in this thesis is the use of inverse theory to determine momentum closure relationships. The momentum relationships are key to understanding the physics of multiphase flow, but more importantly they are the key to understanding (and therefore optimizing) the operational behavior of processes that use gas-solid flows (*e.g.*FCC and pneumatic transport). As discussed above, the momentum closure relationship or momentum exchange terms (MET) are used in two fluid modeling to couple the solid and gas phase momentum equations and in some models couple the solid-solid momentum exchanges [52]. Often these relationships or terms are based on dubious assumptions about the nature of the solid gas interaction (e.g. single particle dynamics). The drag correlations derived from these assumptions are often empirical relationships that depends on a few factors including: solid particle diameter d_p, particle density ρ_p, the void fractions of the solid and gas phases, ϵ_s and ϵ_g, the particle Reynolds number and the velocity difference between the phases $|V_s - V_g|$. For example Symlal and O'Brien derive the following formula for gas-solid interaction.

$$F_{sg} = \frac{3\epsilon_g \epsilon_s \rho_g}{4V_{rm}^2 d_p}(6.3 + 4.8\sqrt{V_{rm}/Re_p})^2(V_s - V_g) \tag{1.6}$$

and

$$F_{ss} = 3(1+e)(\pi/2C_{fm}\pi^2/8)\epsilon sg \tag{1.7}$$

where V_{rm} is the ratio of the terminal velocity of a group of particle to a single isolated particle, and $Re_p = d_p|V_s - V_g|\rho_g/\mu_g$ is the solid phase particle Reynolds number. Now the question arises, can you successfully model multiphase phenomena with so little ability to change the interaction of the solid and gas phases. As it stands, the only operational parameters which differentiate a fluidized bed of sand and a fluidized bed of reactive catalyst are the particles' diameter and density. Is this a plausible assumption given the complex flow phenomena experimental observed? We seek to answer this question (or some part of it) by examining the results of an inverse parameter estimation study. In this study, the MET is parameterized and than estimated from a combination of experimental data and computational modeling. Traditionally, inverse methods have been applied to complex phenomena where the object is to extract vital process or operational information (e.g. oil or strength of material). This is precisely the type of information that would allow operational optimization of multiphase flows. Because inverse methods require experimental a short and related discussion is given of information theoretic methods for design of experiment. Though only tangentially important to the physics of multiphase flows, proper design of experiment is vitally important to most engineers.

1.4.2 The Lagrangian method for dense multiphase flows

As stated previously, Lagrangian methods are generally applied to dilute solid-gas flows, because the of complexity associated with coupling the momentum of the

solid and gas phases and the great computational expense of running simulations with large numbers of particles. Until recently the latter constraint limited these types of simulation to the largest computers. However, with the advent of faster microprocessors, large dense phase Lagrangian simulations have become viable for cluster is of desktop machines. The second part of this thesis examines the use of a mixed numerical scheme; Eulerian gas flow with Lagrangian particles tracking for dense solid-gas flows. The results of the simulation are compared against the experimental results of Tsuji [71] and Durst and Lee [39]. Few computational schemes have been able to reproduce the general trends in Tsuji and Durst and Lee's work.

1.4.3 Conclusion

In this introduction we have provided a basic taxonomy of gas-solid multiphase flows and gave a brief introduction to the two novel subjects to be examined in the remainder of this thesis. The two investigations: inverse parameter estimation in multiphase flows and Euler-Lagrangian methods for dense flows are part of a larger more complex topic – inter-momentum transfer in multiphase equations. The topics presented in this thesis are two "windows" into this poorly understood aspect of multiphase flows. Hopefully, by looking through these windows engineers and scientist will be better able to understood the mechanism of interphase momentum transfer.

Chapter 2

Euler-Lagrangian for dense phase flows

2.1 Introduction

A number of industrial processes involve the flow of particulate materials. Examples include: pneumatic conveying, flow in the riser section of a fluidized bed reactor,polymer processing and stirred tank mixing. Because a clear understanding of the physical mechanisms in these flows is vital to scale-up and design of new processing equipment a great deal of numerical and experimental research has been conducted in this field. Most computer simulations of gas/solid flows can be divided into two categories: Eulerian (continuum) models and Lagrangian models. Eulerian models seek to derive a set of continuum equations in each phase by application of averaging techniques to the instantaneous equations of motion in each phase [28]. The averaging procedure used to obtain the continuum equations also produces a number of ancillary dependences that must be resolved before proper closure of the equation set. These ancillary relationships and the accompanying constitutive equations make the application and interpretation of two fluid models difficult. An alternative to continuum models, and the approach taken in this study, is to use Lagrangian methods.

Lagrangian methods extract the relevant features of the physical system by tracking the motion of the solid particles. The individual particle trajectories are calculated from the forces exerted by the fluid, other particles, and the solid boundaries. Lagrangian multiphase simulation can be divided into two categories based on the mass-loading or particle density of the flow. The first category is the two-way cou-

pled formulation in which the influence of the particles on the fluid phase is taken into account by introducing source terms into the Eulerian fluid equations,thereby coupling the phases. This formulation is important at higher mass loading, where the presence of the solid phase influences the gas phase and visa versa. In the second category, the flow's fluid dynamics determine the particle distribution. Often called one-way coupling, this method is used to model systems in which the mass loading is low (i.e. particle flow interaction are minimal).

Lagrangian methods have a number of advantages over continuum models such as the simplified modeling of multi-size particles and fewer assumptions about the equations. But until recently, the computational expense of Lagrangian methods meant that only a small number of particles could be tracked, severely limiting the applicability of these methods to industrial flows. However, the advent of high-speed multi-processors computers now make Lagrangian simulation a viable alternative to two-fluid models in the dilute to moderately dense phases regimes. This study reports on efforts to understand gas/particle flows through a two-way coupled simulation, the results of which are compared against experimental results. Special emphasis has been placed on computational efficiency and algorithmic generality in order to produce a stable framework in which to conduct these numerical experiments.

Migdal and Agosta [48]were the first to propose combining Lagrangian solid particles and Eulerian fluid mechanics for multiphase flow by showing that particles could be treated as sources of mass and momentum in a fluid field [10] [35]. Since then,

Lagrangian particle methods have been used to study various aspects of gas-solid flows including: particle-fluid turbulence interactions [46] [27] hydrodynamic forces between the solid and fluid phases [44], and particle-particle interactions [72] in dense flow systems. Lun and Liu [42] modeled the flow of particles in horizontal channel coupling the particle and fluid momentum. In the next two sections, we examine the hydrodynamic and collisional interactions of solid particle in a fluid stream.

2.2 The particle equation

In its most general form the equation governing particle motion is:

$$m_p \frac{\mathbf{du_p}}{\mathrm{dt}} = \mathbf{\Sigma F_p} \tag{2.1}$$

where $\mathbf{u_p}$ is the velocity of the particle and $\mathbf{\Sigma F_p}$ is the sum of the forces on the particle. The simple form of this equation belies the complex nature of the particle equation, which in wall-bounded flows can be influenced by a number of factors including: gravity, lift due to fluid shear and particle rotation, particle-wall collision, interparticle collisions, inertial effects, particle metrology and turbulence. The forces that effect the trajectory of the particles are of three types: forces due to the fluid (hydrodynamic), forces due to the presence of the boundaries and interparticle forces.

In this study only the hydrodynamic (including gravity) and interparticle forces are included in the particle equation. The Maxey-Riley [44] expression for forces on

a sphere in a quiescent fluid serves as the basis for the hydrodynamics forces. However, because of the assumptions used in its derivation, the Maxey-Riley expression must be modified and augmented in order to be valid in the flow regimes of interest. Particle-particle interactions become increasingly important as the mass loading (or the particle concentration) increases. With higher mass loading the average time between particle collision is smaller than the average time the particle spends between collisions. Thus the particle has little time to responds to the hydrodynamic forces. Particle-particle interactions also prevent particle concentrations from exceeding the maximum concentration for the physical properties of the particle. The particle equation used in the study is of the form:

$$m_p \frac{\mathbf{du}_\mathrm{p}}{\mathrm{dt}} = \mathbf{F}_\mathrm{d} + \mathbf{F}_\mathrm{l} + \mathbf{F}_\mathrm{vm} + \mathbf{F}_\mathrm{pg} + \mathbf{F}_\mathrm{wall} + \mathbf{F}_\mathrm{coll} + (1 - \frac{\rho_\mathrm{f}}{\rho_\mathrm{p}})\mathbf{g} \tag{2.2}$$

Where $\mathbf{F}_\mathrm{d}$ is the drag forces, $\mathbf{F}_\mathrm{l}$ are the lift forces, $\mathbf{F}_\mathrm{vm}$ is the virtual mass force, $\mathbf{F}_\mathrm{pg}$ is the pressure gradient force, $\mathbf{F}_\mathrm{wall}$ is the wall interaction force and $\mathbf{F}_\mathrm{coll}$ is the collisional force. A cursory review of the particles forces is presented in the next section, and a scaling analysis follows in which the relative magnitude of the forces is compared and equation (2.2) simplified.

2.2.1 Hydrodynamic forces

Drag

Drag is felt by objects as they move through the fluid and is a result of pressure and frictional forces on the objects surface.

$$\mathbf{F}_{\mathrm{d}} = \frac{1}{8}\mathrm{C_d}\pi \mathrm{d_p^2}\rho_{\mathrm{f}}(\mathbf{u_f} - \mathbf{u_p})|\mathbf{u_f} - \mathbf{u_p}| \tag{2.3}$$

Here, C_d is the drag coefficient. The general form of the drag coefficient for a sphere [50] is

$$C_d = \frac{K_1}{Re_p} + \frac{K_2}{Re_p^2} + K_3 \tag{2.4}$$

where K_1, K_2 and K_3 are empirically derived coefficients.

Lift

Lift forces, which act perpendicular to the drag forces, has two principal components. The Saffman lift (F_{ls})due to fluid shearing and the Magnus lift (F_{lm}) due to asymmetric flow

The Saffman lift force is:

$$\mathbf{F_{ls}} = 1.615\mathrm{C_{sm}}(\rho_{\mathrm{f}}\mu_{\mathrm{f}})^{1/2}\mathrm{d_p^2}|\omega_{\mathbf{f}}|^{1/2}[(\mathbf{u_f} - \mathbf{u_p}) \times \omega_{\mathbf{f}}] \tag{2.5}$$

where $\omega_f = (\nabla \times \mathbf{u_f})$ and C_{sm} is the correction to the Saffman original formulation,

in which both the particle Reynolds number, Re_p and the Reynolds shear number, $Re_{sh}(= d_p^2/\nu du_f/du_y)$ are less than one. For Re_p >40; $C_{sm} = .0524(Re_p \frac{d_p}{2|\mathbf{u_f}-\mathbf{u_p}|}|\omega_\mathbf{f}|)$. Implicit in this form of the Saffman lift forces is the assumption that the distance from the particle to the wall is much greater than the particle radius. This assumption plays an important role in the scaling analysis to follow.

The Magnus lift forces is due to asymmetric flow around the particle

$$\mathbf{F_m} = \frac{1}{2}\rho_\mathrm{f}(\mathrm{u_f} - \mathrm{u_p})^2 \frac{\pi \mathrm{d_p^2}}{4} \mathrm{C_{LM}} \frac{(\mathbf{u_f} - \mathbf{u_p}) \times \ \omega_\mathbf{r}}{|\omega_\mathbf{r}|} \tag{2.6}$$

C_{LM} is the lift coefficient and has an approximate value of .5 for dilute suspensions. The spin of the particle relative to fluid

$$\omega_\mathrm{r} = \nabla \times \mathbf{u_p} - .5\nabla \times \mathbf{u_f} \tag{2.7}$$

Virtual Mass Force

When a body is accelerated through a fluid there is an acceleration of the fluid around it. The additional force required to accelerate this fluid is called the virtual mass force. Auton [5] gives the virtual mass force as

$$\mathbf{F}_\mathrm{vm} = \frac{\rho_\mathrm{f}}{2\mathrm{V_p}} \frac{\mathrm{d}}{\mathrm{dt}} (\mathbf{u_f} - \mathbf{u_p}) \tag{2.8}$$

Pressure gradient forces

The pressure gradient force is

$$F_{pg} = \rho_f \frac{D\mathbf{u_f}}{Dt} \tag{2.9}$$

where: $\frac{D}{Dt}$ is the material derivative $= \frac{\partial}{\partial t} + \mathbf{u_f} \cdot \nabla$

2.2.2 Interparticle force

In general, there are two techniques employed for modeling particle-particle interactions in gas-solid flows. The first is the hard sphere model, which is based on the impulsive forces between particles, and the soft sphere model, in which the amount of "overlap" between particles is used to produce a repulsive force [17] [59]. In this study we use the soft sphere model, because of its simplicity and easy of implementation. In the soft sphere model, the interparticle force, F_{coll} is composed of a normal and a tangential force.

$$F_{coll} = F^n_{coll} + F^t_{coll} \tag{2.10}$$

The normal component of the collisional force is of the form

$$\mathbf{F^n_{coll}} = (-\mathrm{k_n}\zeta_{\mathbf{ij}} - \lambda_\mathrm{n}(\mathbf{v_i} - \mathbf{v_j})\mathbf{n_{ij}})\mathbf{n_{ij}} \tag{2.11}$$

where: k_n is the stiffness of contact, ζ_{ij} is called the virtual overlap and defined as

$\zeta_{ij} = d_p - |\mathbf{x_i} - \mathbf{x_j}|, \mathbf{x_i}$ is the (x,y,z) coordinate of the center of mass for particle i (or j), $\mathbf{n_{ij}}$ is the unit normal pointing from particle i to particle j and λ_n is the dissipative constant. The stiffness constant,k_n is calculated from Hertizan contact theory [69],

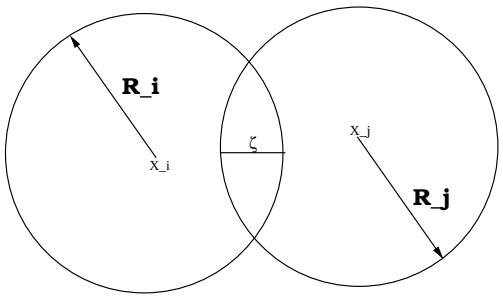

Figure 2.1: The virtual overlap of 2 particles

in which Poisson's ratio,σ_s^2 and Young's modulus, E_s determine the "strength" of the contact between the two particles. According to this theory, the normal component of the collisional force, P_n and the virtual overlap ζ_{ij} are nonlinearly related

$$P_n = K_n \zeta_{ij}^{3/2} \tag{2.12}$$

In the case of two sphere of equal diameter

$$K_n = \frac{\sqrt{2d_p} E_s}{3(1-\sigma_s^2)} \tag{2.13}$$

Substitution of the Hertizan contact force, P_n into the equation 2.11

$$\mathbf{F^n_{coll}} = (-\mathrm{K_n}\zeta^{\frac{3}{2}} - \lambda_\mathrm{n}(\mathbf{v_i} - \mathbf{v_j}) \cdot \mathbf{n_{ij}})\mathbf{n_{ij}} \tag{2.14}$$

The dissipative constant,λ_n can be derived from the critical damping condition of the spring-dashpot-friction slider mechanical system. Tsuji has extended this model by relating the dissipative constant to the materials coefficient of restitution, ϵ_p.

$$\lambda_n = \beta(\epsilon_p)\sqrt{m_p \frac{P_n}{\zeta_{ij}}} \tag{2.15}$$

where β is a function of the restitution coefficient (ϵ_p). For the particles used in this study β=.2 (ϵ_p=.8). The tangential component is of the form:

$$\mathbf{F^t_{coll}} = -f\mathbf{F^n_{coll}}\frac{\mathbf{n_{ij}}}{|\mathbf{n_{ij}}|} \tag{2.16}$$

$f$is the friction coefficient, which is a measurable quantity.

2.2.3 Wall-particle interactions

For wall bound flows, the wall-particle interactions can be an important, especially as it relates to such issues as erosion and nanoparticle fluidization. The particle interacts with the wall through two mechanism. The first mechanism is hydrodynamic interaction due to the proximity of the wall. McLaughlin [46] reviews a number papers in which the hydrodynamic interaction of the wall and particle are studied. These papers suggest several modifications to the horizontal and vertical components of the particle drag coefficient in order to correct for the presence of the wall. In addition to the drag force, McLaughlin examines several modifications to the Saffman lift

term, which in its original form does not include the wall effects. These modification still assume that $l \ll d_p$, where l is the distance between the particle center and the wall. The second mechanism for wall particle interaction is mechanical behavior. Depending its inertia, a particle may collide with the wall or be captured with cohesive force (eg. van der Waals forces). The collision between wall and particle can be modeled with either the hard sphere or soft sphere approach.

2.2.4 Scaling and Non-Dimensional Groups

Scale analysis of the governing equations and hydrodynamics forces provides considerable insight into the behavior (eg. timescale) of the flow. Assume typical values for the parameters in solid/air vertical pipe flow [39] [71]: are: d_p=.03m, $\rho_f \approx 1.2\frac{kg}{m^3}$, $\nu_f \approx 1.5e-5\frac{m^2}{sec}$, $d_p \approx 5e-4m$, $\rho_p \approx 2000kg/m^3$, $\lambda = \frac{u_p}{u_f}$. $m_p \approx 5.5e-7kg$, $A_p \approx 2.01337e{-}6m^2$ than $F_d \approx 3\pi\nu_f d_p \rho_f |u_f(1-\lambda)| + 1.413\nu^{.313} d_p^{1.687} \rho_f |u_f(1-\lambda)|^{1.687}$.

It becomes clear that the importance of the Saffman and drag forces are dependent on two factors: the difference between the particle and fluid velocities ($u_f(1-\lambda)$) and the rate of shear ($|du_f/dy|$). The following criteria must be met for the Saffman and drag forces to be of the same order of magnitude:

$$2432[u_f(1-\lambda)] + 6650[u_f(1-\lambda)]^{.628} \approx |du_f/dy| \tag{2.17}$$

For the bulk of the flow this criteria is never met. However, close to the wall the

relative velocities are small and the shear rate maximum, the issue of whether the criteria above can be met is not so clear. Thus, inclusion of the Saffman lift into the reduced particle equation is problematic. The issue is complicated by the lack of experimental data close to the wall. Based on these factors the Saffman force is not included in the study.

The pressure gradient force, $\mathbf{F}_{\mathrm{pg}} \approx \rho_{\mathrm{f}}/\rho_{\mathrm{p}} \approx 10^{-3}$ and is negligible.

The gravity term, $m\mathbf{g} \approx 5.4\mathrm{e}-6$ is an order of magnitude less than the drag force, but because drag scales as the velocity squared, at lower relative velocities the gravity would be of the same order (or larger) than the drag, and therefore must be included in the final form of the particle equation. The particle equation (1) can now be simplified

$$m_p \frac{d\mathbf{u_p}}{\mathrm{dt}} = \mathbf{F}_{\mathrm{d}} + \mathrm{m_p}\mathbf{g} + \mathbf{F_{coll}} \tag{2.18}$$

The virtual force and Bassett forces are negligible because $\rho_f/\rho_p \approx 10^{-3}$.

In addition to simplifying equation 2.2, scaling analysis aids in the effort to establish parameters that characterize particle motion. For turbulent flow systems, particulate motion depends on a number of factors including: the Stokes number (St), defined as

$$St = \frac{\tau_p}{\tau_f} \tag{2.19}$$

where τ_p is the particle relaxation time(aerodynamic response time) and τ_f is the the

fluid timescale. If the Stokes number $St \ll 1$ than the particles can be expected to follow the flow, similarly for $St \gg 1$ the particle are not influenced by the turbulent flow structure, having insufficient time to response to the fluid fluctuations. The particle timescale scales as , $\tau_p \approx \rho_p d_p^2/18\mu \approx 4.7s$. The fluid timescale is more complicated. A number of fluid timescales can chosen including: viscous, Kolmogorov and large eddy. In pipe flow, the large eddy timescale maybe the most appropriate for the calculation of the Stokes number [25]. Assuming $\tau_f = 0.003s$, St $\approx$ 1500, implying that turbulence does not influence the particles trajectory through the flow. If the viscous timescale is chosen, the Stokes number calculated becomes a measure of the influence of non-homogeneities close to wall on the particle. Young and Hanratty [74] claim that for a viscous Stokes number, St $\geq$ 20-30 wall turbulence is not important. Assuming a viscous timescale, St $\approx$ 100000, implying that wall bound turbulence is not important.

2.3 Fluid Equations

A key element in the application of the Lagrangian method to gas-solid particle dynamics is the numerical methods used to generate the fluid velocity field, which is used as "input" into the particle tracking algorithm (see Figure 2.3 for more detail). The fluid velocity field is generated by solving the Navier-Stokes equation with the appropriate boundary conditions. The Navier-Stokes equations are one of the most studied equations in all engineering and mathematics, and there are a large number

of textbooks and journal articles that cover almost all aspects of the Navier-Stokes including: the numerical techniques that are used to solve the various forms (compressible,incompressible,turbulent etc) of the Navier-Stokes. In the next sections we will review the Navier-Stokes, the influence of turbulence on particle dispersion and finally the incorporation of turbulence into the Navier-Stokes Equation.

2.3.1 The Navier-Stokes Equation

To review: the Navier-Stokes equations (in the x,y,z coordinate system) are of the form: 1. Mass Conservation Equation

$$\frac{\partial}{\partial t}(\rho_f) + \nabla \cdot (\rho_f \mathbf{u_f}) = 0 \tag{2.20}$$

2. Momentum Conservation Equation

$$\rho_f[\frac{\partial}{\partial t}(\mathbf{u_f}) + (\mathbf{u_f}\nabla)\mathbf{u_f}] = \frac{\mathrm{dP}}{\mathrm{dx}} + \nabla \cdot [\mu_\mathrm{f}(\nabla(\mathbf{u_f}))] + \rho_\mathrm{f}\mathbf{g} \tag{2.21}$$

From the scaling arguments above, we know that the flow is incompressible and turbulent. Turbulent flows require that the standard Navier-Stokes be supplemented to account for the dissipative and chaotic effects of turbulence.

2.3.2 Interaction of turbulent flow with solid particles

In this section we will review the effect of turbulence on solid particles. Although, we have concluded from the scaling argument above that the effect of turbulence is relatively minor (given the large Stokes number) for the particles and flows speeds in this study, how turbulence effects small particle (St ≤ 1) dispersion is an important topic and should be reviewed. Shirolkar, Coimbra and McQuay [61] is an excellent review of turbulence and its effect on solid particles. Much of the discussion below is taken from this reference.

Turbulence is the three dimensional macroscopic manifestation of increased vorticity and strain in the flow. Researchers in the area turbulent flows have devised a number of conceptual frameworks in order to understand turbulence. The most widely applied framework uses the concept of an eddy (or the rotating structures found in turbulent flow) to understand how turbulence is generated, how scalar quantities are transported in turbulent flows and how turbulent flows interact with solid objects (e.g. solid particles). This model has a number of assumptions which help to understand and model turbulent flow and its interactions with solid particles including:

1. Eddies of various sizes are present in a turbulent flows.

2. Because large eddies cannot respond to rapidly to viscous forces they are often broken into smaller eddies. This phenomena is called turbulence decay.

3. The process of turbulence decay occurs until viscous forces become dominant.

4. Each eddy has an associated length and timescale known as the eddy length and the eddy lifetime. The eddy length is the physical size of the eddy and eddy lifetime is the time that eddy will maintain its current size.

With the "basic" assumptions out of the way, we can now go on to the more complex issue of the interaction of solid particles and turbulent eddies. The interaction of the solid particle and a turbulent eddy depends on two factors: the inertia of particle and the particle's free velocity. The influence of a particles' inertia was discussed briefly in the last chapter. Infact our discussion of the Stokes numbers was really a discussion of the effects of inertia on particle-eddy interactions (though we didn't frame the argument in terms of inertia explicitly). The second factor effecting a solid-particle eddy interactions is the particle's free fall velocity or terminal velocity, which is an important in the migration of particles from one turbulent eddy (before it decay due to viscous forces) to another eddy. The so-called crossing trajectory effect (CTE) is an important (experimentally verified) feature of turbulent particle flows.

Lagrangian Particle Dispersion Models

The study of solid particle dispersion in a turbulent flow field is an old one (relatively speaking). The first substantive work was done by G.I. Taylor in the 1920's. In Taylor's model (which we will use as a starting point for this discussion), small particles were released in a homogeneous stationary (not a function of time) turbulent

flow. The variance in the fluid particle position (σ_x^2) in one dimension is given as

$$\sigma_x^2 = 2\int_0^{t_1}\int_0^{t_2}\langle(u'_p(t_2)u'_p(t_1))\rangle dt_1 dt_2 \tag{2.22}$$

Where u'_p is the fluctuating part of the particle velocity (more on the this later. For right now assume that a particle's velocity is the sum of a steady velocity, $\langle u_p\rangle$ and a fluctuating velocity u'_p). In order to avoid the problem of estimating the velocity autocorrelation, $\langle(u'_p(t_2), u'_p(t_1))\rangle$ Taylor defined an autocorrelation function that is a function of the time difference (ξ=t1-t2).

$$R^L(\xi) = \frac{\langle u_p(0)u_p(\xi)\rangle}{\langle u_p^2\rangle} \tag{2.23}$$

Substituting (2.23) into 2.22 and simplifying with partial fractions yields:

$$\sigma_x^2 = 2\langle u'\rangle^2\int_0^t (t-\xi)R^L(\xi)d\xi \tag{2.24}$$

If we assume a very form for the autocorrelation:

$$R = \begin{cases} 1.0, & \xi < t_{fl} \\ 0, & otherwise \end{cases} \tag{2.25}$$

Here t_{fl} is called the Lagrangian timescale and is approximately the time interval

over which the fluid is correlated with itself.

$$t_{fl} = \int_{\infty}^{t} R^L(\xi) d\xi \tag{2.26}$$

More intuitively, it can be viewed as the characteristic large eddy lifetime.

Using the Venkatram autocorrelation(2.25) function, we are able to derive two important results. Firstly, if the travel time of the particle is less than the Lagrangian timescale t_{fl} the variance of the fluid particle grows as the square of the time of travel.

$$\sigma_x^2 = \langle u' \rangle^2 t^2 \tag{2.27}$$

When the particle travel time is much less than the Lagrangian fluid time scale, the variance become proportional to the time of travel.

$$\sigma_x^2 = \langle u' \rangle^2 t_{fl} \tag{2.28}$$

The main limitation in Taylor's theory is the assumption that the flow is stationary. Since most turbulent flows are not stationary there have been many efforts to expanded and extend Taylor's result. Shirolkar [61] divides these efforts into four major categories: random walk models, deterministic dispersion models, eddy lifetime models, time-correlated models, and pdf propagation models. Each model is a specific example of a Markov process, that is a stochastic process that relies on situational

probability to transition between states [34]. A short explanation of each model is given below.

Random Walk Models

In the random walk model, a particle's trajectory is defined by two equations;

$$dy = u'_p(t)dt \tag{2.29}$$

and

$$u'_p(t + dt) = R^L(dt)u'_p(t) + RW_p \tag{2.30}$$

RW_p is a normal random variable that can be sampled from a Gaussian probability density function. Equation 2.30 is the finite difference form of the Langevin equation. It can be shown that as dt approaches zero, the autocorrelation function assumes a exponential shape. Thus we are able to validate random walk models with the Taylor's model by using an exponential autocorrelation function,$R^L = e^(|\xi/t_{fl})$.

Deterministic Dispersion Models

In these type of model the fluctuating component of the of the particle velocity u'_p is modeled as

$$u'_p = \Lambda_p \frac{1}{\bar{n}_p} \frac{\partial \bar{n}_p}{\partial x} \tag{2.31}$$

here Λ_p is the particle diffusivity which is the ratio of the turbulent particle viscosity and the turbulent particle Schmidt number. Obviously, this methods suffers from the same parameter estimation problems that the two fluid or continuum methods have.

Eddy lifetime Models

Eddy lifetime models estimate the fluctuating component of the fluid velocity (which is then used to estimate the particle velocity) by randomly sampling from a PDF generate from the local turbulence properties, k and ϵ. For isotropic flows:

$$P(u'_f) = \sqrt{\frac{3}{4k\pi}} exp\left[-\frac{{u'_f}^2}{.75k}\right] \tag{2.32}$$

The fluctuating velocity associated with an eddy is assumed to be constant over the interaction time,τ_i. Knowing the interaction time and the u'_f we can use

$$u_p = u_f + (u_p^{old} - u_f)e^{-\tau_i/t_p} + gt_p[1 - e^{-\tau_i/t_p}] \tag{2.33}$$

Generally, the interaction time,τ_i is

$$\tau_i = min(t_{fl}, t_c) \tag{2.34}$$

Unlike deterministic models, in this procedure particles with the same physical property and initial condition will have necessarily have the same trajectory. Eddy models

are also very good at modeling the crossing trajectory effects (discussed previously).

Time-correlated dispersion models

8 Time correlated dispersion models are similar to eddy lifetime models with that the fluctuating component of the fluid velocity along the particle path now calculated using its value at the fluid particle location and a spatial autocorrelation functions. Unfortunately, even the simplest details of these methods are very complex and the read is referred to works by Berlemont [8] and Burry and Bergeles [21].

PDF propagation models

In PDF propagation model, a PDF represents a group of particles having the same physical properties and initial condition. The particle statistics are extracted from this PDF. In most models of this type, the PDF is assumed to have a Gaussian distribution of the form:

$$p(x,y,t) = \frac{1}{2\pi\sigma_x(t)\sigma_y(t)\sqrt{(1-r^2(t))}} exp - \frac{1}{2(1-r^2(t))} \tag{2.35}$$

$$\frac{x-\nu_x(t)^2}{\sigma_x^2(t)} - 2r(t)\frac{(x-\nu_x(t))(y-\nu_y(t))}{\sigma_x(t)\sigma_y(t)}\frac{y-n_y(t)^2}{\sigma_y^2(t)} \tag{2.36}$$

where: r(t) = $\frac{\sigma_{xy}}{\sigma_x}\sigma_y$, ν_x is the ensemble mean particle location and σ_{ij} is the particle covariance relationship (which can be related to R^L the particle correlation tensor. The full expressions are given in Shirolkar [61].

In reviewing the theoretical foundation of the most recent models for particle-turbulence it becomes clears that this issue is still a very active and potentially fruitful area of research. In the author's opinion, many of the models shown (in spite of there complexity) lack a firm foundation. A more rigorous first principles approach (perhaps starting from statistical mechanics) may provide additional insight into the problem of solid particle-turbulence interaction.

2.4 Numerical Methods

In the previous section, we examined the effect of turbulence on small particle dispersion. As we noted previously, for the particles and flows under consideration turbulence is of secondary importance. But secondary importance does not mean of no importance, and we must take great care in selecting a turbulence modeling approach which works on both a theoretical and practical (implementation) level. Bardina [6] divides the techniques for predicting turbulent flows into six categories.

1. Correlations.

2. Integral equations.

3. One point closure models.

4. Two point closure models.

5. Large eddy simulation.

6. Direct numerical simulation.

The most commonly used technique to model turbulent flow are point closure models. The most common type of one point closure model is the Reynolds Averaged Navier-Stokes. The RANS techniques is ubiquitous and used in a number of commercial packages. In this approach the fluid velocity are divided into two parts: steady and unsteady, this "new velocity" is substituted back into the Navier-Stokes and then averaged. The resulting equations require an additional set of equation to close the equation set. In the next sections, we will review how the Navier-Stokes equations are averaged, and the RANS equations constructed.

2.4.1 Preliminaries

In this approach the fluid velocities are first divided into two components a steady and two components a steady and an unsteady component.

$$u_f = \bar{u}_f + u'_f \tag{2.37}$$

where $\bar{u}_f$ is the steady fluid velocity and u'_f is the unsteady component of velocity. Equation 2.37 is then substituted into the governing equations and averaged. The averaging function is defined

$$\bar{\phi} = \lim_{T\to\infty} \frac{1}{T} \int_0^T \phi(x,t)dt \tag{2.38}$$

Because equation 2.38 is a linear operator, its application to linear terms is straightforward. For example if equations 2.37 and 2.38 are applied to the diffusive momentum term, $\nabla(\nabla \cdot \mathbf{u})$ the resulting equation $\nabla(\nabla \cdot \bar{\mathbf{u}})$ has exactly the same form as the non-averaged equation. Only how the equation is interpreted changes. However, when 2.37 and 2.38 are applied to a nonlinear equation (eg. convective scalar flux) the resulting averaged equation has additional terms. The additional terms generated by the averaging procedure are problematic and require additional equations in order to 'close' the equation set. To illustrate how averaging a nonlinear expression may produce additional terms a quadratic term is averaged.

$$u_f \phi = (\bar{u}_f + u'_f)(\bar{\phi} + \phi') \tag{2.39}$$

$$(\bar{u}_f + u'_f)(\bar{\phi} + \phi') = (\bar{u}_f \bar{\phi}) + (\bar{u}_f \phi') + (u'_f \bar{\phi}) + (u'_f \phi') \tag{2.40}$$

Now, 2.40 is averaged.

$$\overline{(\bar{u}_f \bar{\phi}) + (\bar{u}_f \phi') + (u'_f \bar{\phi}) + (u'_f \phi')} = (\bar{u}_f \bar{\phi}) + \overline{(u'_f \phi')} \tag{2.41}$$

Just to clarify, the simplification above, let's review some of the properties of the average function and make clear the some of the assumption used. We assume that the average of the fluctuating component is zero ($\bar{\phi}' = 0$). The last term on the right hand side is zero only when u'_f and ϕ' are uncorrelated. This term $\overline{(u'_f \phi')}$ is called the

turbulent scalar flux. In the RANS momentum equations, when ϕ' is equal to v'_f, the resulting term $\overline{(v'_f u'_f)}$ is called the Reynolds stresses. The Reynolds stresses are the heart of RANS modeling and are the source of the "closure problem" in turbulence modeling. In the RANS model the Reynolds stress terms can take two forms: the eddy viscosity model and the Reynolds stress model. Eddy viscosity models relate the Reynolds stresses $\overline{(v'_f u'_f)}$ to the mean velocity gradients and a mean turbulent diffusion (μ_t). Eddy models are classified by the number of partial differential equations which must be solved in order to compute the turbulent diffusion. Zero equation (or algebraic models) compute the turbulent diffusion directly from the local mean flow quantities. Examples of algebraic models are the Prandtl mixing length model and constant viscosity models.

In two equation models like the k-ω and k-ϵ, two additional partial differential equations are required to close the Navier-Stokes. Reynolds stress models avoid the turbulent stress tensor terms by using individual equations for the individual turbulent stresses. Reynolds stress models use separate transport equations for each tensor component

2.4.2 The Reynolds averaged Navier-Stokes equations

Substitution of 2.38 and 2.40 into the Navier-Stokes yields the equations below. These are the Reynolds averaged Navier-Stokes [14]. Please note: in order to account for the mass and momentum of the solid phase the density is multiplied by the solids

volume fraction, β. All the quantities below are time-averaged. Only the fluctuation component is shown. The time-averaged continuity equation:

$$\frac{\partial}{\partial t}(\beta_f \rho_f) + \frac{\partial}{\partial x_i}(\beta_f \rho_f \mathbf{u_f}) = 0 \tag{2.42}$$

The time-averaged momentum equation:

$$\frac{\partial}{\partial t}(\beta_f \rho_f \mathbf{u_f}) + (\mathbf{u_f} \cdot \nabla)(\beta_\mathrm{f} \mathbf{u_f}) = \nabla \cdot [\mu_\mathrm{f}(\tau_\mathbf{ij} + \tau'_\mathbf{ij})] + \beta_\mathrm{f} \rho_\mathrm{f} \mathbf{g} + \mathbf{S_p} \tag{2.43}$$

$\beta_f = (1 - n_p V_p / V_f)$. Equation (2.43) has the same form as the standard momentum equations with the velocities now representing time-averaged values and the incorporation of turbulence through the "Reynolds-stresses", $\tau'_\mathbf{ij}$. The mean fluid stress tensor is:

$$\tau_\mathbf{ij} = \mu(\nabla \mathbf{u_f} + \nabla \mathbf{u_f^t}) \tag{2.44}$$

and the Reynolds stress tensor is :

$$\tau'_\mathbf{ij} = -\frac{2}{3}\rho_\mathrm{f} \mathrm{k} \delta_\mathrm{ij} + \mu_\mathrm{t}(\nabla \mathbf{u_f} + \nabla \mathbf{u_f^t}) \tag{2.45}$$

where k is the turbulent kinetic energy. The Reynolds stress tensor is analogous to the shear stresses that arise in laminar flow, with exception of the turbulent viscosity μ_t. The form of the turbulent viscosity is proportional to the product of the turbulent

velocity and length scales.

$$\mu_t = \rho_f C_\mu \frac{k^2}{\epsilon} \tag{2.46}$$

The values of the k and ϵ are obtained by solution of the following conservation equations:

$$\frac{\partial}{\partial t}(\rho_f k) + \nabla \cdot (\rho_f k \mathbf{u_f}) = \nabla \cdot \left((\frac{\mu_\mathrm{t}}{\sigma_\mathrm{k}}) \nabla \mathrm{k} \right) + \mathrm{R_k} - \rho_\mathrm{f} \epsilon \tag{2.47}$$

$$\frac{\partial}{\partial t}(\rho_f \epsilon) + \nabla \cdot (\rho_f \mathbf{u_f} \epsilon) = \nabla \cdot \left(\frac{\mu_\mathrm{t}}{\sigma_\epsilon} \nabla \epsilon \right) + \mathrm{C_1 R_k} \frac{\epsilon}{\mathrm{k}} - \rho_\mathrm{f} \mathrm{C_2} \frac{\epsilon^2}{\mathrm{k}} \tag{2.48}$$

where R_k is the rate of turbulent kinetic energy production

$$R_k = \mu_t (\nabla \mathbf{u_f} + \nabla \mathbf{u_f^t}) \nabla \mathbf{u_f} \tag{2.49}$$

$C_1, C_2, C_\mu, \sigma_k$ and σ_ϵ are empirical constants with values of 1.44, 1.92, .09,.1.0,1.3 respectively. The Reynolds averaged fluid equations above are solved with a collocated finite volume code [29]. Unlike standard finite volume methods, this method collocates velocity and pressure at same position. This collocation of variables provides a tractable approach to the exchange of momentum that is required in dense particulate flows.

2.4.3 Momentum Exchange between Phases

The one of the most difficult problems in multiphase flow is understanding how non-collisional momentum is transferred between phases. This momentum transfer for sufficiently dense flows couples the phases. It is this coupling that produces the interesting hydrodynamics of the fluidized bed. As stated above, one of the factors that motivates the use of particle simulations for dense gas/solid flows is that momentum exchanges reveals itself more naturally as a byproduct of the drag and lift forces, rather then a explicit term in the Navier-Stokes equations. There are a number ways in which to couple the gas and solid phases, one of the most popular being the particle source in cell (PSI-cell)method [19].

$$S_{PSI-cell} = \frac{n_p m_p}{V_c} \frac{\Delta V}{\Delta T} \tag{2.50}$$

Here ΔV is the change in velocity of particle between the entrance to a control volume and its exit, and ΔT is the time takes the particle to travel through the control volume.

2.4.4 Finite Volume Method

Like most numerical methods the finite volume method seeks to replace the continuous values of an analytic solution to a differential equation with approximate or discrete values. The process of replacing the continuous with the discrete is called discretization. In the case of the finite volume method the continuous solution do-

main of the differential equation is subdivided into a finite number of control volumes surrounding a grid point. The differential equation is integrated over each control volume producing a set of algebraic equations connecting the independent variable(s) (or scalar variables in the case of the generalized transport equation) and grid points. As the number of grid points increases, the finite volume method approaches the analytic solution.

According to Patanker [67] the most attractive feature of the finite volume method is that solution of the derived discretized equations imply a integral conservation of quantities such as mass,momentum and energy over any group of control volumes. In the next few sections the discretization process for a generalized transport equation is illustrated. The goal is to familiarize the reader with the basic concept of the finite volume methods, which will later be applied to the more complex Reynolds Averaged Navier-Stokes.

2.4.5 The general transport equation

Assume a conservation equation of the form

$$\nabla \cdot (\rho \mathbf{u} \phi) = \nabla \cdot (\Gamma \nabla \phi) + \mathrm{S}_{\phi} \tag{2.51}$$

Where ϕ is a scalar quantity (eg. temperature,pressure,concentration). The solution domain of over which we wish to solve this equation is then discretized or subdivided

into a finite number of small control volumes. As the geometry of the solution domain becomes more complex; how that domain is discretized becomes increasingly important. In the finite volume method, the integral form of equation 2.1 is generally used as the starting point for the discretization of the governing equation. We begin the finite volume formulation by integrating Equation 2.51 over a generalized control volume:

$$\int_V \nabla \cdot (\rho \mathbf{u} \phi) \mathrm{dV} = \int_{\mathrm{V}} \nabla \cdot (\Gamma \nabla \phi) \mathrm{dV} + \int_{\mathrm{V}} \mathrm{S}_\phi \tag{2.52}$$

A general method for the approximation of the spatial integral terms in the scalar transport equation (2.52) is outlined below:

1. The volume integral is converted to surface integral by application of the divergence equation

$$\int_V \nabla \cdot \mathbf{f} \mathrm{dV} = \int_{\mathrm{S}} \mathbf{f} \cdot \mathbf{n} \mathrm{dS} \tag{2.53}$$

2. The surface integral is the sum of the integrals over each face,k of the control volume.

$$\int_S \mathbf{f} \cdot \mathbf{n} \mathrm{dS} = \sum_{\mathrm{k}} \int_{\mathrm{S_k}} \mathbf{f} \cdot \mathbf{n} \mathrm{dS_k} \tag{2.54}$$

3. The flux,F through a single face is approximated using the appropriate interpolation method. In the next section steps 1-3 are used with each term of the scalar transport equation to generate an approximation, which will be used to solve the transport equation.

Transient term

Integrating the transient term over a control volume leads to the approximation

$$\int_{t}^{t+\delta t} \int_{V} \frac{\partial(\rho\phi)}{\partial t} dV dt \tag{2.55}$$

If the control volume,V does not change in time the order operation of the integral can be changed and V can be neglected.

$$\int_{t}^{t+\delta t} \frac{\partial(\rho\phi)}{\partial t} dt \tag{2.56}$$

There are several methods to approximate (or discretized) the time derivative. In general the time discretization can be divided into two categories: explicit discretization and implicit discretization. The key difference between the two categories is the stability criterion or the rate at which the system is allowed to progress in time. Generally, implicit schemes allow larger time stepping and evolve the system faster.

Convective Term

The convective term is:

$$F^{c} = \int_{V} \nabla \cdot (\rho \mathbf{u} \phi) \mathrm{dV} \tag{2.57}$$

using the methodology outline above. The convective flux through the kth face is

$$F_k^c = \int_{S_k} \rho\phi\mathbf{u}\cdot\mathbf{n}\mathrm{dS_k} \approx \mathrm{m_k}\phi_\mathrm{k} \tag{2.58}$$

where m_k is the mass flux through the 'kth' face of the control volume. Because the faces of the control volume lie between computational nodes (or nodes where values are known) interpolation must be used to approximate their values. Numerous interpolation schemes are available; two of the most popular schemes are linear (CDS) and upwind(UDS). How interpolation is used in the approximation of the convective flux is shown in the illustrated example below.

Diffusive Term

The diffusive term is

$$F^d = \int_V \nabla\cdot(\Gamma\nabla\phi)dV \tag{2.59}$$

Using the methodology outlined above the diffusive convective through the 'k' face can be approximated

$$F_k^d = \int_{S_k} \Gamma\nabla(\phi)\cdot\mathbf{n}\mathrm{dS_k} \approx \Gamma\left(\frac{\partial\phi}{\partial\mathrm{n}}\right)_\mathrm{k} \tag{2.60}$$

2.4.6 Illustrated example in 2-D

Using the control volume shown below

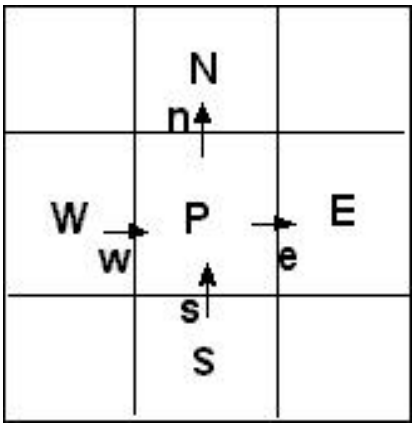

Figure 2.2: Control volume

The convective and diffusive fluxes can be approximated through any of the faces of the control volume. For illustrative purposes assume that we are interested in the 'e' face of the control volume. The other faces can be integrated in a similar manner.

$$F_e^c = \int_{S_k} \rho\phi\mathbf{u}\cdot\mathbf{n} \approx \mathrm{m_e}\phi_\mathrm{e} \tag{2.61}$$

where m_e is the mass flux through the 'e' face.

$$m_e = (\rho u_x)_e \Delta y \tag{2.62}$$

Because the velocities are known only at the cell centers (ie. E,W,N,S), we must use interpolation to evaluate the velocity at the cell faces. If we use the UDS or CDS

interpolation the convective flux becomes:

$$F_e^c = \begin{cases} max(m_e, 0)\phi_P + min(m_e, 0)\phi_E, & UDS \\ m_e(1-\lambda_e)\phi_P + m_e\lambda_e\phi_E & CDS \end{cases} \tag{2.63}$$

$\lambda_e = x_e - x_P/x_E - x_P$. The UDS approximation satisfies the boundness criteria unconditionally, that is they never yield oscillatory solutions,however they are numerically diffusive,meaning that areas in which variables change rapidly will be smeared out. CDS schemes can yield oscillatory solutions but is the simplest second order scheme.

The diffusive flux is evaluated with CDS interpolation of the normal derivative;

$$F_e^d = \Gamma \left(\frac{\partial \phi}{\partial n}\right)_e \Delta y = A_e^d(\phi_E - \phi_P) \tag{2.64}$$

where $A_e^d = \frac{\Gamma \Delta y}{x_E - x_P}$.

If we extend the example and 'loop' over all the faces of the control volume. Then the equation for a generic node P is:

$$A_W\phi_W + A_S\phi_S + A_P\phi_P + A_N\phi_N + A_E\phi_E = S \tag{2.65}$$

if A_k is the sum of the convective and diffusive flux coefficient $A_k^c + A_k^d$.

$$\begin{aligned} A_E^d &= \tfrac{-\Gamma\delta y}{x_E - x_P} & A_W^d &= \tfrac{-\Gamma\delta y}{x_W - x_P} \\ A_N^d &= \tfrac{-\Gamma\delta y}{x_N - x_P} & A_S^d &= \tfrac{-\Gamma\delta y}{x_S - x_P} \\ A_P^d &= -\textstyle\sum_k A_k^d \quad k = E, W, N, S \end{aligned} \tag{2.66}$$

Depending on the interpolation scheme used the convective flux coefficients may be:

For UDS:

$$\begin{aligned} A_E^c &= min(m_e, 0); & A_W^c &= min(m_w, 0) \\ A_N^c &= min(m_n, 0); & A_S^c &= min(m_s, 0) \\ A_P^c &= -\textstyle\sum_k A_k^c & k &= E, W, N, S \end{aligned} \tag{2.67}$$

For CDS:

$$\begin{aligned} A_E^c &= m_e\lambda_e & A_E^c &= m_w\lambda_w \\ A_N^c &= m_n\lambda & A_E^c &= m_s\lambda_s \\ A_P^c &= -\textstyle\sum_k A_k^c & k &= E, W, N, S \end{aligned} \tag{2.68}$$

If we evaluate equation 2.65 at all of the nodal points in the discretized domain a linear system can be generated, which when solved gives the value of the scalar quantity at each of the nodal points. In equation 2.51 the velocity of the fluid that convects the scalar quantity is known apriori. In the case where the velocity of the fluid is unknown the the methods above must be extended to solve the Navier-Stokes equations. The pseudocode below shows how the general transport equation is solved

on a computer. An actually working (very important) example can be found at ftp.springer.de/pub/technik/peric. The codes used by Peric form the basis the codes used in this study.

```
Setup grid x[i:num_in_x],y[i:num_in_y];
Read physical properties
// coordinate of cell centers
do i = 2:num_in_x-1
xc[i] = .5*(x[i]+x[i-1])
end
do j = 2:num_in_y-1
yc[j] = .5*(y[j]+x[j-1])
end

// Initalize variables
do i = 2:num_in_x
do j = 2:num_in_y
fi[i,j] = 0
end
end

// Inital values
do j = 2:num_in_y
                fi[1,j] = 1 - yc[j]-ymin/(ymax-ymin)
        end
// calculate mass fluxes at cell face
do i = 1:num_in_x -1
        do j = 2:num_in_y-1
        cu[i,j] = density*x[i]*(y[j]-y[j-1])
        end
        end


do i = 1:num_in_y - 1
        do j = 2:num_in_x - 1
                cv[i,j] = density*y[i]*(x[j]-x[j-1])
        end
        end
```

```
do j = 2:num_in_y - 1
dw[j] = -diff_const*(y[i]-y[i-1]/(xc[2] - xc[1])
end

do i = 2:num_in_x - 1
asd = -diff_const*(x[i]-x[i-1]/(yc[2] - yc[1])
// Loop over the control volume
// Calculate diffusional part of transport equation
   do j = 2:num_in_y - 1
        awd = dw[j]
   aed = -diff_const*((y[j] - y[j-1])/(xc[i+1])-xc[i])
and = -diff_const*((x[j] - x[j-1])/(yc[i+1])-yc[i])
// Calculate convection part
     if (UDS)
aec  = min(cu[i,j],0)
awc  = -max(cu[i-1,j],0)
anc = min(cv[i,j],0)
asc = -max(cv[i-1,j],0)
     if (CDS)
aec = cu[i.j]*fx[i]
awc = -cu[i-1,j] *(1-fx(i-1))
anc = cv[i.j]*fx[i]
asc = -cv[i-1,j] *(1-fx(i-1))
// Add diffusional and convective parts
ad[i,j] = aed + aec
aw[i,j] = awd + awc
an[i,j] = and + anc
as[i,j] = asd + asc
ap[i,j] = -(ae[i,j]+aw[i,j]+an[i,j]+as[i,j])
q[i,j] = 0
  end
end

Impose boundary conditions

Solve System of Equations
```

2.5 The FVM for the Navier-Stokes

In the previous section, the various terms of the generalized transport equation are approximated. The approximations (and the techniques used to generate them) can be applied to the Navier-Stokes equations. There are however several substantiative differences between the Navier-Stokes and transport equations. Firstly, the velocity field is assumed to be a give in the transport equations, in the Navier-Stokes equation the velocity field is what is being solved for, Secondly, the pressure term in the Navier-Stokes has no analog in the transport equation and lacks an independent equation. And finally, the algebraic systems generated by the Navier-Stokes is non-linear, thus the straightforward solution of the previous section is now an iterated process. The primary challenge in the application of the FVM to the Navier-Stokes equations lies in the lack of an explicit equation for the pressure. The solution algorithm used to solve the NS equations must overcome this problem. A number of algorithms are available which address this problem, one of the most popular being the SIMPLE (Semi-Implicit Method for Pressure-Linked Equations) family of algorithms.

2.5.1 The SIMPLE Algorithm

The SIMPLE algorithm recasts the continuity equation in terms of a pressure correction calculation and is normally performed on a staggered grid (see figure below). The staggered grid is used because of problems coupling the pressure and velocity fields. The sequence of operations for the SIMPLE algorithm:

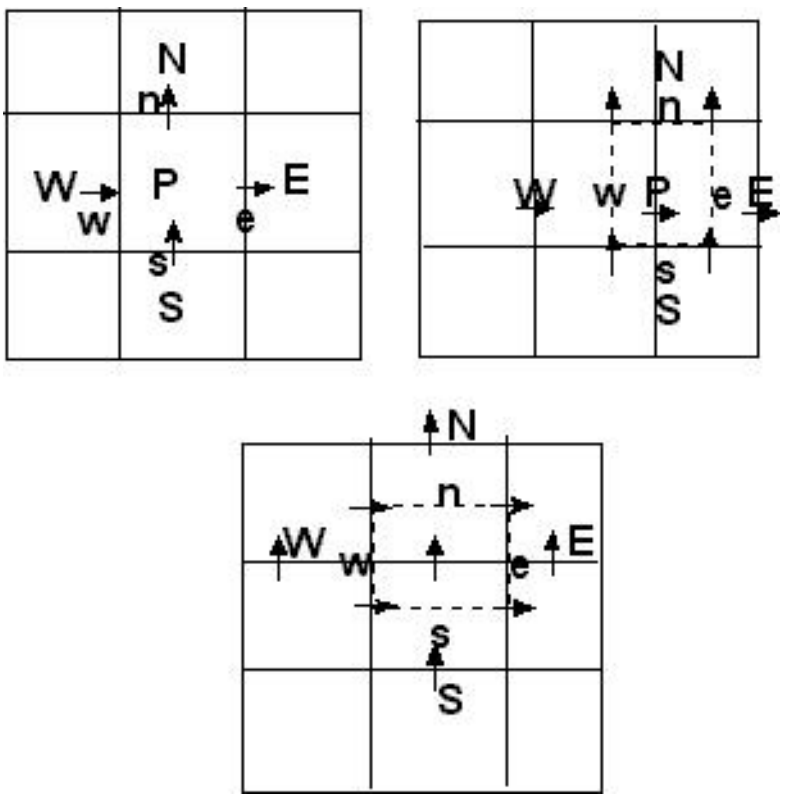

1. Guess the pressure field p^*.

2. Solve the discretized equations to obtain u^* and v^* based p^*

$$\left(\frac{\Delta x \Delta y}{\Delta t} + \sum_l A_l^u\right) u_P^* + \sum_l A_l^m u_l^* = -b^u - \Delta y(p_e - p_w) \tag{2.69}$$

The coefficients for the equation are:

$$
\begin{aligned}
A_E^u &= min(m_e^u, 0) - \tfrac{\mu_e S_e}{x_E - x_P} \\
A_N^u &= min(m_n^u, 0) - \tfrac{\mu_n S_n}{x_N - x_P} \\
A_W^u &= min(m_w^u, 0) - \tfrac{\mu_w S_w}{x_W - x_P} \\
A_S^u &= min(m_s^u, 0) - \tfrac{\mu_s S_s}{x_S - x_P} \\
A_P^u &= A_P^t - \textstyle\sum_l A_l^u; l = E, W, N, S
\end{aligned}
\tag{2.70}
$$

$$
\left(\frac{\Delta x \Delta y}{\Delta t} + \sum_l A_l^v \right) v_P^* + \sum_l A_l^m v_l^* = -b^v - \Delta x (p_n - p_s) \tag{2.71}
$$

The coefficients for the equation are:

$$
\begin{aligned}
A_E^v &= min(m_e^v, 0) - \tfrac{\mu_e S_e}{y_E - y_P} \\
A_N^v &= min(m_n^v, 0) - \tfrac{\mu_n S_n}{y_N - y_P} \\
A_W^v &= min(m_w^v, 0) - \tfrac{\mu_w S_w}{y_W - y_P} \\
A_S^v &= min(m_s^v, 0) - \tfrac{\mu_s S_s}{y_S - y_P} \\
A_P^v &= A_P^t - \textstyle\sum_l A_l^u; l = E, W, N, S
\end{aligned}
\tag{2.72}
$$

3. Solve the pressure correction equation

$$
\nabla^2 p' = \frac{1}{\Delta t} \nabla \cdot u^* \tag{2.73}
$$

4. Calculate "corrected velocities"

$$u^c = -\frac{1}{\Delta t}\nabla p' \tag{2.74}$$

5. Solve for misc scalar variables (ie. temperature,concentration and turbulence)

6. Calculate the next guessed pressure

$$p^*_{new} = p^*_{old} + p' \tag{2.75}$$

7. Return to step 1 until converged solution is obtained

2.6 Assumptions and Algorithms

Assumptions based on the previous sections:

1. Fluid turbulence has very little effect on the particle paths.

2. The fluid velocity has reached steady state.

3. Particle motions are uncorrelated except for particle-particle interactions.

4. Drag is the only hydrodynamic force present.

These assumptions are used to develop the algorithms used in the simulation. In general, most Lagrangian simulations can be done in three parts. Firstly, the solution

of the continuum fluid equations. Second, solution of the equation of motion for each particle. And finally the coupling between phases. For dilute systems this final step can neglected. However, if the phases are coupled, the flow field is recalculated with a source term generated by the particulate phase. This process continues until convergence. Schematically:

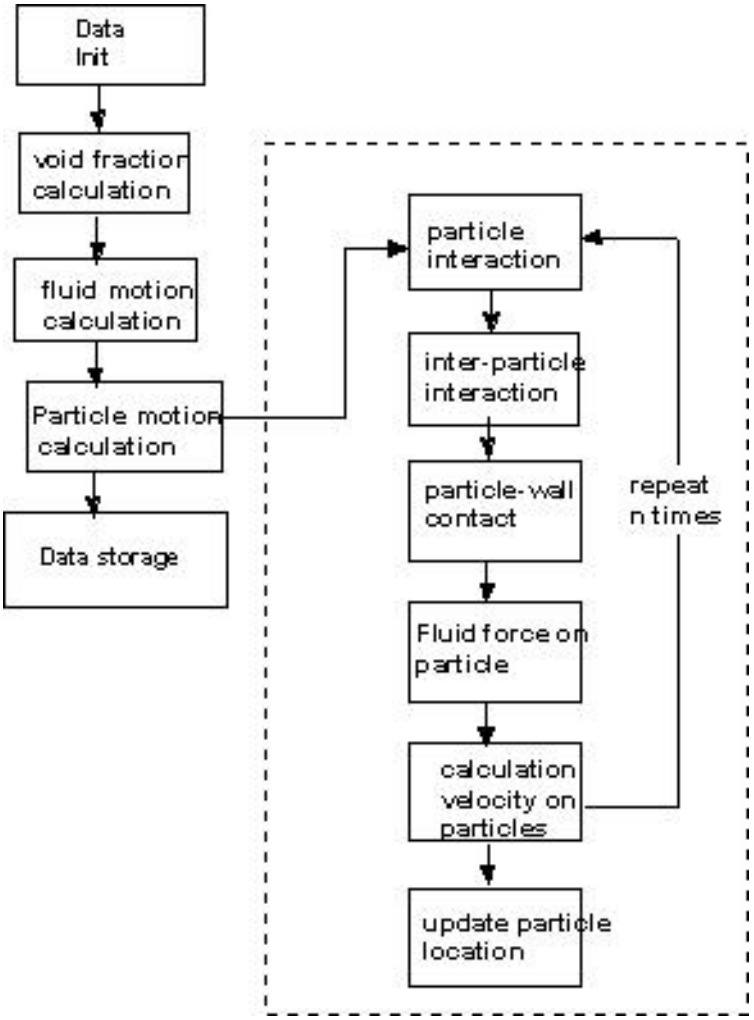

Figure 2.3: Lagrangian simulation flowchart

The particle equation calculations done in this paper are similar to those done in Molecular Dynamics (MD) studies of liquids and solids [3]. Therefore, the numerical and data management techniques developed in Molecular Dynamics provide an excellent starting point for algorithm selection. A number of particle integration schemes where studied included Stormer-Verlet and Gear predictor corrector. Although more computational expensive a fourth order Runge-Kutta scheme was selected to solve the particle equation. As is the case with MD calculations, the particle collision, specifically determining which particle pairs can collide takes much longer than the integration scheme. Thus a great effort was placed into finding an an optimal data structure to hold fluid cell and particle information. Because of the number of particles and the type of calculations, the ability to work effectively on parallel computers is vital. The computer platform chosen was a SGI Origin2000, a 128 processor and shared memory parallel computer. The shared memory nature of the platform further complicates the issues, because fluid and particle data can be global to all the processors. The fluid cell data structure held geometry (e.g. the cell's nodal coordinates, nodal velocities,volume, nearest neighbors) and particle information. The particle information was chained together in a doubly linked list. As the particles move through the domain, they are add (or subtracted) from the entering cells particle list. The master process uses the number of particles in the cell to load balance the parallel calculation. Because particles can only collide with those in the same cell, the determination of collisional pair is greatly simplified. Because the fluid velocity at the

particle's current position is required to calculate the hydrodynamics forces, the fluid cells are isoparameterically mapped from the physical domain to a computational domain where linear interpolation of the fluid velocity at a point is easier [57].

In the next section, a number of comparisons are made to LDV experimental data. Because, particle and fluid data is available everywhere in the flow data, not just at specific points in the flow, an averaging technique to "boil down" the data was employed. At a selected distance downstream of the pipe entrance, a virtual measurement cross-section is setup. As particles pass through this cross-section, their velocity and position as a function of distance from the pipe wall are measured. After the simulation is over, the particle positions are grouped into a number of bins, and an average bin velocity is calculated. Thus, as the number of bins increase the "resolution" of the calculation is increased.

2.7 Results and Discussion

The results of the numerical computation are compared against the experimental results of Tsuji et al. [71]. Tsuji reported data for gas/solid flows in a vertical pipe using laser Doppler velocimetry. The solids used in the experiment were polystyrene spheres of varying diameters ranging from 200μ m to 3 mm with a density $\rho_s = 1030\frac{kg}{m^3}$. In this paper, comparisons are made with two specific diameters 200μm and 500 μ m particles. The glass vertical pipe used to convey the particles was 5 m long with an ID=30.5 mm. An effort was made to model the entire length of the pipe.

Because of the severe pipe diameter to pipe length ratio, special care was necessary in order to achieve convergence and stability. A grid sensitivity study was conducted in order to determine a grid size which gave a grid independent solution for the experimental pipe diameters. A grid size of 200 by 50 was determined to be sufficient. As with any study that attempts to compare numerical results with experimental data, a "point to point" comparison of data is difficult because of the innumerable factors which influence both experiments and numerical calculations. A more realistic goal is to numerically mimic the experiments with an eye towards matching the dominant trends and then understanding the influence that key parameters have on those trends.

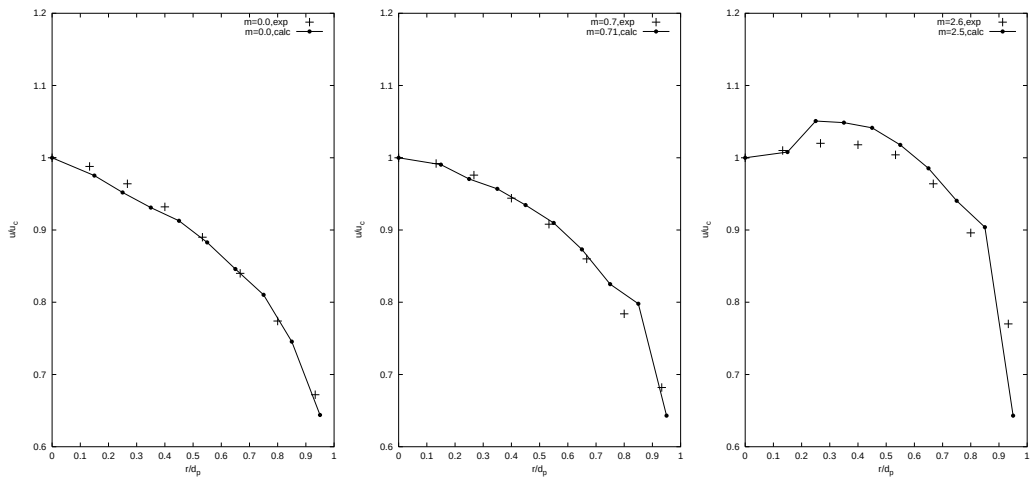

Figure 2.4: (a) Mean air velocity distribution in the presence of 500 μ m at (a)m=0.0 (b) m=0.7 (c) m=2.5

Figures 2.4 (a)-(c) present comparisons of the predicted gas velocity with the experimental results of Tsuji for 500 μm particles. The best agreement with experiment is at low mass loading. At lower mass loading the importance of the particle/particle

interaction and the pipe wall/particle interactions is much smaller. The computational model captures the essential trends in the data the most important of these being the concavity of the air velocity profile as mass loading increase. Also as expected, the heavy particles reach a slower terminal velocity.

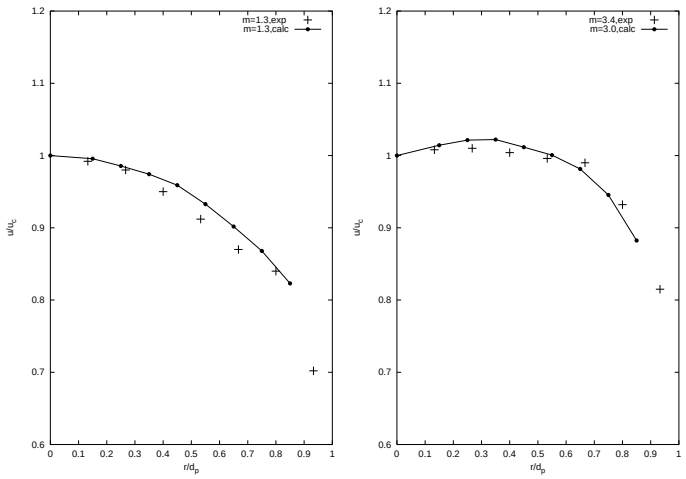

Figure 2.5: Mean air velocity distribution in the presence of 200 μ m at (a) m=1.3 (b) m=3.0

In figures 2.5 (a),(b) comparisons of the air velocity profiles for 200 μm are presented. The velocity profiles for the 200 μm particles show a slight concavity at higher mass loadings, this shifting of the maximum centerline velocity is not as pronounced as the 500 μm case for approximately the same mass loading. The shift of the maximum velocity is a result of the size and functional form of the momentum exchange term used to couple phases. As the momentum exchange, which is the source-term in the fluid momentum equations, increases we see a greater deviation from normal fluid behavior (ie. fluid velocity is a maximum at the pipe centerline). In both cases the computational results deviated most significantly near the wall. This was due in

large measure to the simple particle/wall interaction. the lack of grid refinement near the wall in the study and potential the non-inclusion of the Saffman lift force.

Axial velocities for 500 μ m particles as a function of distance from the centerline are shown below in figure 2.6. The results compare poorly with the experimental particle velocities. However, the computational results follow same trend as the experimental result, that the particle velocity increases with mass loading.

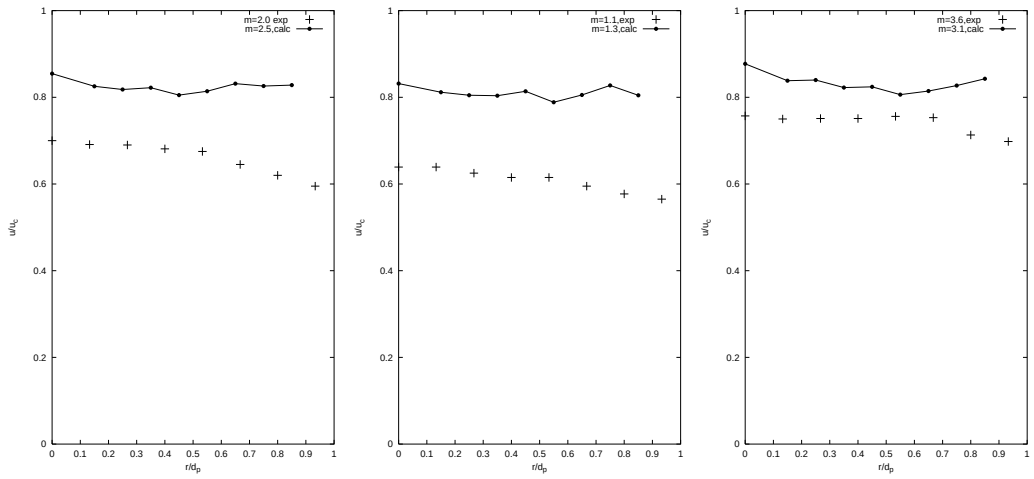

Figure 2.6: 500 μ m particle velocity distributions for different mass loading (a) m=1 (b) m=1.1, (c) m=3.1

It is interesting to note that a range of values (150-12000) for the particle/particle stiffness constant, k_n were tested, including a value derived from Hertzian contact theory. The results of the calculation turned out to be relatively insensitive to the values of k_n chosen. Although the amount of time to solution convergence did change significantly depending the value. This was an obvious by-product of the numerical methods used to solve the particle equations.

Perhaps the most interesting feature of the Tsuji (and Lee and Durst) data is the asymmetry at higher mass loading. This type of symmetry breaking has important implications for Our simulations show this feature, but do not answer the question – Why does this happen? Perhaps, the best way to look at this problem is analytically. This is not an easy task given the nonlinear nature of the problem. But there are some intriguing simplifications that can be made to the problem. Firstly, let us reduce the dimensionality and eliminate the time dependence. This is similar to the approach taken by Jean and Peddieson [38] (more on this later). The problem now looks like

$$U_f \frac{\partial U_f}{\partial x} = -dp/dx + \nabla \cdot U_f + (U_f - U_p)^2 \tag{2.76}$$

Equation 2.76 is the viscous Burger's equation with an additional nonlinear term $(U_f - U_p)^2$ representing the quadratic drag term. In its current form it is difficult to get an exact or analytic solution. However, we can make a few preliminary observations: In equation 2.76 there two terms that could potentially effect flow's symmetry: the nonlinear source term and the convective term.

- The nonlinear term is in the first approximation an even function, which would not break a flow's symmetry. We can illustration this easily, by setting U_p and the convective term equal to zero and solving, a "simple" nonlinear ODE.

$$-dp/dx + \nabla \cdot U_f + (U_f)^2 = 0 \tag{2.77}$$

with boundary conditions

$$U_f(0) = 0; U_f(L) = 0; \tag{2.78}$$

Using a perturbation analysis with no-slip conditions at the boundary, we find that the resulting equation does not submit an asymmetrical solution. The solution is a quadratic with even higher order terms (U^6), which will only flatten the gas velocity profile at higher flow rates. So, have we missed something? Based on this simple analysis all we can say is that the nonlinear term (forcing function) contributes only to the flatness of the velocity. Is it possible that a momentum (or drag) term does not effect the flow symmetries, this also implies that the momentum terms cannot effect particle segregation or other hydrodynamic phenomena. This begs the question Is the drag term $(U_f - U_p)^2$ really an even function? Intuition tells us that the addition of the particle velocity function

- If we substitute a linear convective term $c\frac{\partial U_f}{\partial x}$ and remove the nonlinear term. We get

$$c\frac{\partial U_f}{\partial x} = -dp/dx + \nabla \cdot U_f = 0 \tag{2.79}$$

Solving this equation, we get:

$$\frac{U_f = dp/dxPexp(cx)}{exp(cP - 1) * c)} \tag{2.80}$$

2.8 Conclusion

A Lagrangian study of solid particles in a turbulent pipe was done. We found agreement between the computational and experimental for particle velocity data. The fluid phase data compared less favorably. However, without the error bars on the experimental data, it becomes difficult to measure the success (or failure) of the calculations. Thus, seek to mimic the predominant trends in the experimental data. Most of the major flow phenomenon where captured, including the shifting of the maximum centerline velocity with increased mass loading and decreasing slip velocity with reduction in particle size.

The bulk of this paper is devoted to the construction and running of a computer simulation for dense phase Lagrangian flows. Each section [of this paper]has been an attempt to justify the model assumptions (e.g. forces acting on the particle, particle-particle interactions,etc) and in an effort to build a case for the validity of the simulation. The general assumption used in most computer simulations is that by justifying (and sometimes validating) each step of the simulation that the overall simulation will be correct. And with this validated simulation we can make predictions about the behavior of the system. The predictive ability of computer simulation is the main justification for there existence. But most computer simulations lack the ability the provide insight into the "nature" of the problem. Turning knobs on a

computer model (parametric analysis) is very different from turning the knobs of the phenomena itself. So rather than "turn the knobs" (change a coefficient here and there) in the simulation, we turned to an hybrid simulation-experimental-analytic approach. By comparing and contrasting simulation,experiment and analytic results we able to show that the Lagrangian method is a valid technique for the dense gas-solid flows.

Chapter 3

Inverse Parameter Estimation

3.1 Background and Motivation

Many important scientific problems require the estimation of parameters in partial differential equations. These inverse or parameter estimation problems arise in several different and diverse areas of science including: heat transfer [54], geophysics [66], aerodynamics [73], ground water flow [36] and acoustics [15]. In this study we examine the feasibility of applying inverse techniques for parameter estimation in multiphase flows, specifically gas-solid fluidized bed, which play an important role in a number of industrial applications including fluidized catalytic cracking of hydrocarbons, mixing of gases, extraction of products from ores, drying solid particles, solids mixing, and coating of metallic parts [26].

Current computational models of fluidized beds rely heavily on empirical and semi-empirical relationships to relate mass,momentum, and energy transfer in the flow. Many of these empirical and semi-empirical expressions use gross approximations and assumptions about the flow, which may result in inaccuracies. In this study, inverse methods are used to estimate and investigate momentum exchange in multiphase models. The section is divided into roughly three parts: 1) a brief introduction to inverse methodology, 2) the hydrodynamics of dense multiphase systems, and 3) application of inverse techniques to parameter estimation in fluidized beds and 4) application of information theory to the optimization inverse methods. Associated with inverse problems are questions of understanding and describing the information content of the measurement, and the relationship between the true state of the system

and that retrieved using inverse methods. R.V. Alifanov [2] notes that "The essence of the inverse problems is to create substance from shadow and is necessarily more complex". It is this "complexity" which we hope to examine, in an effort to motivate the use of inverse techniques to dense multiphase systems.

3.2 Inverse Methodology

Consider the equation

$$y^{''} + [k^2 - q(x)]y = 0 \tag{3.1}$$

The normal or direct solution of the equation (with boundary conditions) can be stated as: Given the function q(x) find the solution y(x,k) satisfying certain prescribed boundary conditions. This is called the forward problem. The inverse problem is the reverse, given certain data(ie. experimental data) associated with solution y(x,k), determine the function q(x). In general, the unknown (in this case q(x)) can be estimated in two ways: parameter and functional estimation. The most commonly employed method and the one used here is parameter estimation. In parameter estimation a parametric form for q(x) is guessed (i.e. $q = Ax + Bx^2$). The objective then becomes determination of A and B.

In the case were the data associated with the y has no experimental error, it would be sufficient to have only 2 data points in order to estimate A and B. However, most experimental data has some noise, which requires additional data points. These

additional points over determine the linear system associated with the solution of the forward problem.

One way of solving an overdetermined set of equations is the least-squares approach. The inverse problem can now be thought of as optimization problem which seeks to minimize an objective function, R, which describes the difference between the calculated values of y and the experimental values of y subject to certain constraints. The appeal of this approach lies in the well-developed theory for optimization. However, DuChateau [23] notes that the solution of the optimization problem may not solve the original inverse problem, because the objective function may be based on data which may not uniquely determine the coefficients. The fundamental difficulty in the solution of inverse problems is the ill-posed nature of the problem. A problem is considered ill-posed if it lacks one of three properties: [55]

1 Existence of the solution.

2 Uniqueness of the solution (i.e. there is at most one solution).

3 Stability of the solution (i.e. the solution depends continuously on the data).

With regard to the last point, solutions are typically quite sensitive to data and indeed many of the difficulties associated with obtaining an experimentally-based inverse solution are due to the ubiquitous uncertainty associated with data. In order to address these issues, most researchers use apriori information to regularize the solutions [2]. Regularization seeks to incorporate information such as smoothness,

boundedness and monotonicity into the inverse procedure.

The parameter identification problem associated with the estimation of momentum exchange can be formulated as an inverse problem; the goal in this case is to determine the coefficients of the momentum exchange term (MET) by minimizing the difference between experimental and calculated data. Gavrus [30] identifies the three steps in a parameter identification problem as follows:

1. Formulation of the forward problem including derivation of the governing equations and numerical techniques used to the solve

2. Definition of the experimental measurements to be used in the parameter identification procedure

3. Estimation of the parameters through optimization of a carefully selected objective function.

The third step is shown in greater detail in figure 1. The process is iterative with the solution of the direct problem constituting the most time-consuming part of the process. The criteria used to select of the optimization scheme and associated limitations is described later.

3.3 The Fluidized Bed

Due to their suitability as mixing devices for heat and mass transfer, fluidized beds are widely used in the chemical process industries. A fluidized bed is a large

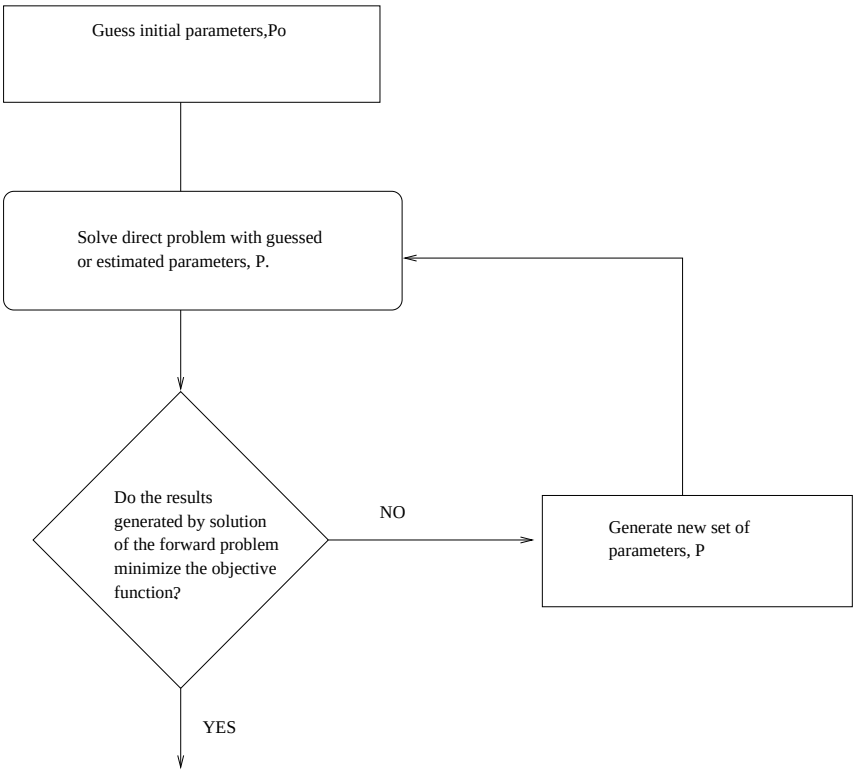

Figure 3.1: Outline of the inverse algorithm

open vessel containing granular material (e.g. catalyst,sand) which is supported by a plate spanning the bottom of the vessel. Generally, the plate is porous and gas is forced upward through it. As the gas flows through the bed, the solid and gas phases interact. These interactions are complex, manifesting themselves in a number of hydrodynamic phenomena [40]. One of the most important of these phenomena is called fluidization, in which the initially stationary particulate bed starts to flowrate reaches a certain value. At this critical value, called the fluidization velocity, the bed expands slightly and the particulate become mobile or "fluidized". As the gas

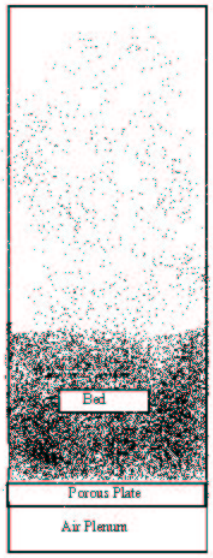

Figure 3.2: Schematic of a fluidized bed

flowrate increases, the bed transitions through a number of interesting hydrodynamic states. Because of the commercial importance of fluidized beds, researchers have spent considerable time and effort in order to understand/model these phenomena and their impact on product quality and process efficiencies. Central to this work is formulation of proper continuum models of fluidized bed systems and accurate estimation of associated momentum exchange terms. The following section describes the most widely used continuum models and highlights how the model is closed through the use of momentum exchange terms.

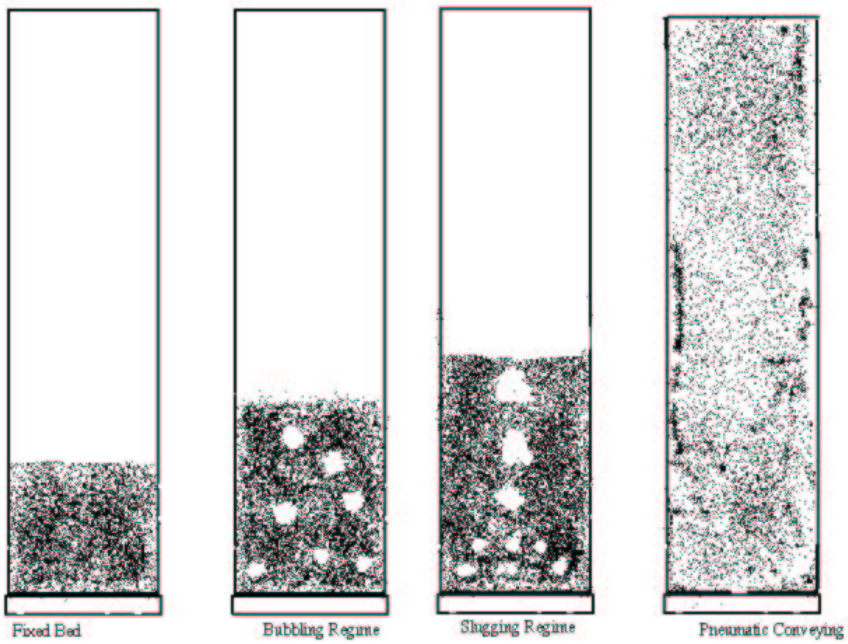

Figure 3.3: Transition points in a fluidized bed

3.4 The hydrodynamics of dense gas-solid flows

Continuum models of multiphase flows derive a set of mass,momentum and energy conservation equations in each phase by application of averaging techniques to the instantaneous equations of motion for each phase [28]. The averaging procedures (see Appendix A) used to obtain the continuum equations also produce a number of ancillary dependencies between dynamic and thermodynamic variables which must be resolved for proper closure of the equation set. One such dependency is the momentum exchange between the solid and gas phases, which we examine below. Understanding the interaction between phases is one of the major challenges in modeling multiphase

flows. Several authors discuss the multiphase continuum equations in detail [31] [62]. The solution of the multiphase equations comprises the direct/forward problem of the inverse problem to be solved. The multiphase equations resemble the single phase Navier-Stokes. It is this resemblance that is used to produce numerical results.

3.4.1 Governing equations

Mass conservation in each phase is governed by

$$\frac{\partial}{\partial t}(\epsilon_m \rho_m) + \nabla \cdot (\epsilon_m \rho_m \mathbf{u_m}) = 0 \tag{3.2}$$

where ϵ_m is the volume fraction of phase m [=(f)luid or (s)olid], ρ_m is the density of phase m, and u_m is the velocity of phase m.

Fluid Momentum conservation is described by

$$\frac{\partial}{\partial t}(\epsilon_f \rho_f \mathbf{u_f}) + (\mathbf{u_f} \cdot \nabla)\epsilon_f \rho_f \mathbf{u_f} = -\epsilon_{\mathrm{f}} \nabla \mathrm{P_f} + \nabla \cdot \tau_{\mathrm{f}} + \epsilon_{\mathrm{f}} \rho_{\mathrm{f}} \mathbf{g} - \mathrm{K_{fs}}(\mathbf{u_s} - \mathbf{u_f}) \tag{3.3}$$

where $\frac{\partial u_j}{\partial x_i}$, μ_f=viscosity of the fluid, μ_s=viscosity of the solid, $\mathbf{u_f}, \mathbf{u_s}$ =fluid and solids velocity, K_{fs} = fluid-solid momentum exchange term, P_f= the gas pressure, τ_f= the gas phase stress tensor.

Conservation of momentum in the solid phase is governed by

$$\frac{\partial}{\partial t}(\epsilon_s \rho_s \mathbf{u_s}) + (\mathbf{u_s} \cdot \nabla)\epsilon_s \rho_f \mathbf{u_s} = -\epsilon_{\mathrm{s}} \nabla \mathrm{P_g} + \epsilon_{\mathrm{s}} \rho_{\mathrm{s}} \mathbf{g} + \mathrm{K_{fs}}(\mathbf{u_f} - \mathbf{u_s}) + \mathrm{K_{ss}} + \nabla \cdot \mathrm{S_{sf}} \tag{3.4}$$

where S_{sf} =the solid phase stress tensor and K_{ss} is the solid-solid interaction term.

One of the most commonly used forms of the momentum exchange term K_{fl} is given below for two different volume fraction ($\epsilon_f \leq 0.8$ and $\epsilon_f \geq 0.8$).

When $\epsilon_f \leq 0.8$

$$K_{fl} = \frac{\mathbf{A}(\epsilon_{\mathrm{f}}^2 \mu_{\mathrm{g}})}{\epsilon_{\mathrm{f}} \mathrm{d}_{\mathrm{p}}^2} + \frac{\mathbf{B}\rho_{\mathrm{g}}\epsilon_{\mathrm{s}}|\mathbf{u_f} - \mathbf{u_s}|}{\mathrm{d_p}} \tag{3.5}$$

When $\epsilon_f \geq 0.8$

$$K_{fl} = \mathbf{C} C_d \frac{\epsilon_f \epsilon_s \rho_g |\mathbf{u_f} - \mathbf{u_s}|}{V_r^2 m d_p} \epsilon_f^{\mathbf{D}} \tag{3.6}$$

Note A,B,C and D have been introduced as a means of parameterizing K_{fl} for use in the inverse procedure. Parameterization of the momentum exchange term allows us to reduce the parameter space for the inverse procedure. The empirically determined values of the remaining constants in (3.4.2) and (3.6) are as follows:

$$C_d = \frac{24}{Re_p}[1 + .15 Re_p^{.687}]; Re_p \leq 1000 \tag{3.7}$$

$$C_d = .44; Re_p \geq 1000 \tag{3.8}$$

$$Re_p = \frac{\epsilon_{sl} \rho_f |\mathbf{u_f} - \mathbf{u_s}| d_p}{\mu_f} \tag{3.9}$$

3.4.2 Interphase Momentum Exchange

In the previous section we touched briefly on the exchange of momentum between phases in multiphase flow. In the opinion of the author, the exchange of momentum between phases is the most underdeveloped and least understood part of multiphase flows. In paper after paper equations like (3.4.2) and (3.6) are used to close the Eulerian multiphase equations without any justification for the parameters or equations chosen. Solid particles in a fluid stream are subject to a number of different forces including drag, lift, Bassett, Faxen, gravity, Magnus and collisional forces. In the Lagrangian approach the interphase momentum transfer was a direct result of solving the particle equation with the appropriate boundary conditions, and the division between hydrodynamic and collisional forces was a clear one. The Eulerian approach to interphase momentum transfer is less explicit and more empirical. Inaddition to taking into account the forces mentioned above, the momentum exchange models used in continuum equations must incorporate a number of other factors including:

1. "The effect of the proximity of other particles must be accounted for. This most important effect implies that the drag force is a function of the solids volume fractions,...."

2. "The above formulations for fluid-solids drag deal with uniform, smooth spherical particles, whereas practical fluid-solids systems contain rough, non-spherical particle of different sizes. A narrow particle-size distribution may be charac-

terized by an average size based on particle surface area... Efforts to study the effect of non-sphericity and roughness on drag are ongoing, and there are no well-accepted ways of treating such effects"

3. "It may be necessary to explicitly account for the effect of particle interactions on the fluid-solid interactions, although equation contains implicit assumptions that the fluid-particle and particle-particle forces can be separated into two terms. For example, the averaging required to approximate the particles as a granular continuum renders the hydrodynamic equations incapable of resolving the wake-dominated micro-hydrodynamics near the particles ... "

Solid-gas interactions

In equations 3.4 and 3.3, the term K_{fs} is the solid-gas exchange term. Unlike Lagrangian methods, which explicitly enumerate the various forces acting on the solid particles, Eulerian methods are incapable of accounting for these different forces explicitly. Continuum momentum exchange terms rely on empirical correlations like the Ergun and Richardson-Zaki equations to model the solid-gas exchange. For example, equations (3.4.2 and 3.6) are empirically derived correlations commonly used to model the gas-solid exchange. Equation 3.4.2 is the parameterized form of the Ergun equation for packed beds, and equation 3.6 is a parameterized form of the Syamlal and O'Brien equation (which itself is a form of the Richardson-Zaki equation [**?**]). The Richardson-Zaki (RZ) equation is a correlation for terminal velocity in fluidized

or settling beds. As we can see, equations and are not so much general purpose momentum exchange correlations, but an interpolation between limiting cases – Ergun for packed beds and RZ for dilute flows.

Continuum momentum exchange terms also suffer from numerical problems caused by ill-posedness. Lyckowski [43] has shown that when the buoyancy force ($-\epsilon_f \nabla P_f$) is included in the fluid momentum equation, all numerical solutions are unconditionally unstable. The notion that a buoyancy force causes the solution to become ill-posed is troubling to say the least and speaks volumes about the "start of the art" in multiphase modeling.

Solid-Solid Interactions

Because continuum multiphase model are primarily used to model dense phase particle collision dominated flows, an understanding of how granular solids interaction is important [4] [65]. In the next section we will discuss classification of granular flows based on the Bagnold number, and how solid particle "exchange" momentum and dissipate energy in a continuum framework. Solid particles interact (dissipate energy and transfer momentum) in three ways depending on the concentration (mass loading).

- Kinetic interaction.
- Collisional interaction.
- Frictional interaction.

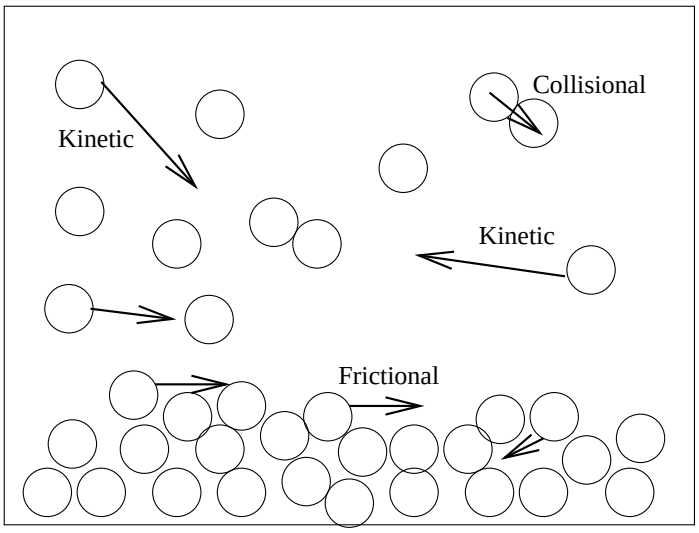

Figure 3.4: Three types of viscous dissipation in a granular flow – kinetic,collisional and frictional

The total stress for granular flows (see equation 3.4) can be divided into two parts based on the type of interaction.

$$\mathbf{S_s} = \mathbf{S_s^f} + \mathbf{S_s^{k,c}} \tag{3.10}$$

The kinetic-collisional tensor $S_s^{k,c}$ is a rate dependent stress tensor due to the momentum transfer during random particle motion and collision,and the frictional tensor S_s^f is rate independent and caused by the rubbing and rolling of particle against one another.

Generally, stress tensors are divided into two parts: a pressure component and a viscous stress component.

$$S = PI + \tau \tag{3.11}$$

here $\mathbf{I}$ is the unit stress tensor. Now casting equation 3.10 into the form of equation 3.11 we get:

$$S_{sf} = P_s I + \tau_{\mathbf{s}} \tag{3.12}$$

P_s is called the solids or particle pressure. This solids pressure is the pressure ($\mathbf{F}$ /A) on the surface of vessel due to the presence of the particulate phase on the multiphase mixture. Now dividing the solid stress based on the two types of interactions. We get

$$S_{sf} = (P_{k,c} + P_f)\mathbf{I} + (\tau_{\mathbf{k,c}} + \tau_{\mathbf{f}})3.4.2 \tag{3.13}$$

Depending on the mass loading, S_{sf} can either be kinetic-collision dominated or friction dominated. We may generalize

$$S_{sf} = \gamma(\epsilon)(P_{k,c} + \tau_{\mathbf{k,c}}) + \mathbf{1} - \gamma(\epsilon)(\mathbf{P_f} + \tau_{\mathbf{f}}) \tag{3.14}$$

Here $\gamma(\epsilon_f)$ is a function weighting factor that "selects" the type of stress. In many multiphase theories a switch (at a critical voidage fraction, ϵ_g^*) is used to choose between kinetic/collisional and frictional interactions. For example in the MFIX

code the solid stress tensor is

$$S_{sf} = \begin{cases} P_{k,c}I + \tau_{k,c} & \epsilon_g < \epsilon_g^* \\ P_f I + \tau_f & \epsilon_g > \epsilon_g^* \end{cases} \quad \textbf{??} \tag{3.15}$$

In fluidized bed simulations, the switch voidage is often set to the void fraction at the minimum fluidization. The full derivation of the solid stress tensor is beyond the scope of this paper, however we can review some the relevant principles of granular flow, in order to make the discussions to follow more clear. In dilute flows, the primary means of the momentum transfer is through kinetic and collisional motion. While for more dense flows, the momentum transfer is controlled by the frictional interaction of the particles.

The kinetic-collisional stress tensor

The kinetic-collisional stress tensor S_k was derived by analogy with the kinetic theory of gases. Like the kinetic theory gases, the kinetic theory of granular materials assumes that the particles are in constant and chaotic motion. The particles are said to have a temperature, a granular temperature that is proportional to its kinetic energy.

$$\Omega_p = const < u_p > \tag{3.16}$$

The "thermodynamic pressure" of a granular material can be defined as $P_{k,s} = \epsilon_p \rho_p \Omega_p$ in direct analogy with the ideal gas law. However, unlike an ideal gas granular

materials do not have a negligible volume, therefore some corrections need to be made to the pressure equation above. These correction are normally done through the addition of the radial distribution function g_o, which gives the probability of finding two particles in close proximity and a material's coefficient of restitution. With these additions the pressure equation is:

The pressure,$P_{k,s}$ is

$$P_{k,s} = 2(1+e)\rho_p g_o \epsilon_p^2 \Omega_p \tag{3.17}$$

The second term in is the granular stress terms, $\tau_{k,c}$. This stress term is defined as:

$$\tau_{k,c} = 2\mu_{p,f} D + \lambda tr(D)\mathbf{I} \tag{3.18}$$

here D is the strain rate tensor $D = \frac{1}{2}[\nabla u_p + \nabla(u_p)^T]$, $\mu_{p,f}$ is the shear viscosity of the solid phase (or the bulk viscosity), and λ_p is the second coefficient of viscosity.

The frictional stress tensor

The stress that arise from frictional interparticle forces are usually modeled by application of plasticity and critical state theory. Similar to functions used in plastic flow theory, an arbitrary function that limits the amount of compressibility in the solid phase is called the solids pressure, P_f

$$P_f = A\epsilon_{sm}(\epsilon_f - \epsilon^*) \tag{3.19}$$

Typically, A = 10^{25} and n = 10 The stress tensor, τ_f is based on critical state theory. In this formulation

$$\tau_f = 2\mu_s D_s s \tag{3.20}$$

where $\mu_s = \frac{Psin\phi}{2\sqrt{(I_2)}}$ and I_2 is the second invariant of the deviator of the strain rate tensor.

If that this point all this makes sense to you.. well you are one smart (or sick) cookie.

Ostensibly the purpose of this section was to review interphase momentum transfer in multiphase flow. However, this section was also designed for more subversive role – to highlight the fact that the current state-of-the-art in the multiphase model is built on a very shaky foundation. It becomes pretty clear in this "review" that interphase momentum transport is a mish-mash of ideas taken from: solid mechanics, soil mechanics, kinetic theory, fluid mechanics, plasticity, and critical state theory. A cobbled to together in a crazy patchwork quilt.

The main motivation for this dissertation is to "work" around the "problem" of interphase momentum transfer. Rather than use a momentum transfer term of dubious origin or applicability, we assume a form for the momentum transfer than fit parameters – we believe this to be a pragmatic solution to a difficult problem.

3.5 Numerical Methods

Perhaps because of its resemblance to the single phase Navier-Stokes, the algorithm used to solve the multiphase fluid equations(3.2) is similar to the SIMPLE algorithms for Navier-Stokes. However, because of the more complex nature of the flow a number of issues need to be addressed before extending the SIMPLE algorithm to multiphase systems [63]. Firstly, there are more field variables and hence more equations. Secondly, there is no unique pressure correction equation for the multiphase Navier-Stokes equations, and finally since the multiphase momentum equations are strongly coupled through the momentum exchange terms, making this term fully implicit is essential. However, to make the exchange term implicit all the equations for each velocity component must be solved together. An alternative is to use a method like the Partial Elimination Algorithm (PEA) [63] to decouple or partially decouple the fluid and solid phase equations.

The multiphase SIMPLE algorithm is more complicated than single phase SIMPLE Algorithm and has many more steps. Rather then go through each step of the algorithm (Syamlal and O'Brien [52] [53] go into excruciating detail) we will briefly outline the steps and cover only the key differences between the multiphase and single phase algorithms.

The Extended SIMPLE Algorithm for Multiphase Flows

1. At the start of the timestep, calculate the physical properties,exchange coefficients and reaction rates.

2. Calculate velocity fields with the current pressure field p^*

$$\left(\frac{\Delta x \Delta y}{\Delta t} + \sum_l A_l^u\right) u_P^* + \sum_l A_l^m u_l^* = -b^u - \Delta y(p_P - p_E) + K_{fl}(u_s^* - u_f^*)_P \quad (3.21)$$

$$\left(\frac{\Delta x \Delta y}{\Delta t} + \sum_l A_l^v\right) v_P^* + \sum_l A_l^m v_l^* = -b^v - \Delta x(p_N - p_S) + + K_{fl}(u_s^* - u_f^*)_P \quad (3.22)$$

As expected the discretized equations 3.21 and 3.22 are coupled through the momentum exchange term K_{fl}. In order to solve the equations efficiently, they must be (at least) partially decoupled. Syamlal and O'Brien [52] use the PEA method of Spalding [63].

The Partial Elimination Method

PEA assumes a transport equations of the form:

$$\epsilon_f \rho_f \frac{\partial \phi_f}{\partial t} + \epsilon_f \rho_f u_f \frac{\partial \phi_f}{\partial x} = 000 \frac{\partial}{\partial x}\left(\Gamma \frac{\partial \phi_f}{\partial x}\right) + F_{fs}(\phi_f - \phi_s) \quad (3.23)$$

$$\epsilon_s \rho_s \frac{\partial \phi_s}{\partial t} + \epsilon_s \rho_s u_s \frac{\partial \phi_s}{\partial x} = \frac{\partial}{\partial x}\left(\Gamma \frac{\partial \phi_s}{\partial x}\right) + F_{sf}(\phi_s - \phi_f) \quad (3.24)$$

if equations 3.23 and 3.24 are discretized the following algebraic equations are generated.

$$(A_f\phi_f)_P = \sum_l (A_f\phi_f)_l + b_f + \Delta V F_{fs}[\phi_s - \phi_f]_P \tag{3.25}$$

$$(A_s\phi_s)_P = \sum_l (A_s\phi_s)_l + b_s + \Delta V F_{sf}[\phi_f - \phi_s]_P \tag{3.26}$$

Note that $F_{sf} = F_{fs}$. When $F_{sf} \to 0$ the two equations are decoupled and

$$(\phi_f)_P = \frac{\sum_l (A_f\phi_f)_l + b_f}{A_{fP}} \tag{3.27}$$

As $F_{sf} \to \infty$ than the equations are tightly coupled and

$$(\phi_f)_P = \frac{\sum_l (A_f\phi_f)_l + b_f + \Delta V F_{fs}(\phi_s)_P}{(A_f)_P + \Delta V F_{fs}} \tag{3.28}$$

Now substituting into 3.26

$$\left[\frac{(A_f)_P + A_s \Delta V F_{sf}}{A_s + \Delta V F_{fs}}\right](\phi_f)_P = \sum_l (A_f\phi_f)_l + b_f + \frac{\Delta V F_{sf}}{A_s + \Delta V F_{fs}}\left(\sum_l (A_s\phi_s)_l + b_s\right) \tag{3.29}$$

3. Calculate fluid pressure correction,P'.

$$\sum_l A_l P'_{gP} = \sum_l A_l P'_{gl} + b \tag{3.30}$$

4. Update fluid pressure field applying an under-relaxation

$$P_g = P_g^* + \omega_{pg} P_g' \tag{3.31}$$

5. Calculate the gradients for use in the solid volume fraction correction equation.

   .

6. Update solid volume fractions. Under-relax in regions where the solids are densely packed and the solid volume fractions is increasing.

$$\epsilon_m = \epsilon_m^* + \omega_{ps} \epsilon_m \tag{3.32}$$

7. Calculate the void fraction.

8. Calculate the solid pressure from the equation of state.

9. Normalize the residuals and check for convergence. If not converged goto Step 1.

3.5.1 Validation of Results

As we have noted previously, proper solution of the forward or direct problem is necessary in order to solve the inverse parameter estimation problem. In order to solve the forward problem in this study we chose to use a modified version of the MFIX code from the National Energy Technology Center in Morgantown,WV. MFIX

is one of the most advanced simulation packages for multiphase flow available. In addition, it is also one of the most validated [11]. MFIX has been compared against a number of experimental studies including: Yang and Kearins, Schmidt,He and the Foster Wheeler Development Corporation 10" Carbonizer Experimental RunTR8.9. MFIX correctly predicted many of the experimental observed phenomena including: bubble formation, jet penetration length, solid circulation cells and transitions to different flow regimes. As with most computer models experimental data comparisons, the results are not perfect. For example, MFIX does not predict the bubbling frequency correctly (too high) and the flow regime transitions are displaced from the experimentally determined conditions.

3.6 Optimization

Due to the nonlinear nature of the governing equations, the corresponding inverse problem is also nonlinear, and thus must be recast as an optimization problem. The appeal of this approach is that the theory and methods of optimization are well developed. However, care must nevertheless be taken in the selection of the objective function and regularization terms, since the data on which these terms are based may not uniquely determine the MET coefficients [23]. There are a number of important issues that need to be considered when selecting the optimization technique for a particular inverse problem including: 1) the size of the parameter space, 2) the time required to evaluate the objective function, 3) robustness of the optimization method

and 4) the computational overhead. In gas-solid fluidization, the size of the parameter space is large and thus the time taken to evaluate the objective function can be enormous.

Due to the inherent complexity of these problems and the large amount of time necessary to calculate the gradients of the objective function, gradient-based methods have not been attempted in this study. Instead, we have evaluated a number of non-gradient techniques including genetic algorithms [32], the principal axis method [13] and the downhill simplex method [56] [47]. These tests show that the simplex method generally exhibits superior stability and faster convergence and thus was used in all numerical experiments described below. The Nedler-Mead simplex method is examined in detail in the section. Of course, the rate of convergence and stability are strong functions of the initial guess and the objective function. After some experimentation, the following objective function was defined:

$$Q = \sum_{i=1}^{N} \beta(\epsilon_i^{exp} - \epsilon_i^{calc})^2 - R \tag{3.33}$$

where ϵ_i^{exp} is the ith experimentally observed void fraction, ϵ_i^{calc} is the corresponding calculated void fraction, N is the number of points where the void fraction is experimentally measured, β=1000 and R is a first-order regularization term given by $R = \frac{1}{2}|\epsilon_i^{exp} - \epsilon_i^{calc}|$. Note that first order regularization is chosen based on the expectation that ϵ_i^{exp} is a fixed constant.

The simplex method

The downhill simplex method was first proposed by Nelder and Mead [51]. The methods seeks to minimize (or maximize) a function f without computing the gradient. The method begins by construction of a simplex, or geometrical figure with N+1 vertices The simplex is then iterated through the solution space by a series of operations. There are four possible operations reflection,expansion,contraction and shrinkage each associated with a scalar parameter. The coefficients of reflection,expansion,contraction and shrinkage are denoted by ρ (not to be confused with fluid density), χ,γ and σ respectively. The standard choices for these parameter are : $\rho = 1, \chi = 2, \gamma = 0.5, \sigma = 0.5$

1 A single new vertex replaces the worst point of the simplex and the iterations continue

2 If a shrink is performed a new set of n points together with x_1 (the best point) form the simplex at the next iteration.

Wright [47] outlines the steps in a Nelder-Mead iteration:

1. Order

   Order the n+1 vertices to satisfy $f_1^{(k)} \leq f_2^{(k)} < \ldots \leq f_{n+1}^{(k)}$. Where $f_i^{(k)}$ is equivalent to $f(x_i^{(k)})$ (or the evaluation of the function f at the point $x_i^{(k)}$ Here the best point in the simplex is denoted $x_1^{(k)}$ the worst is $x_{n+1}^{(k)}$.

2. Reflect

   Compute the reflection point, x_r from

$$x_r = \bar{x} + \rho(\bar{x} - x_{n+1})$$

   where $\bar{x}$ is the centroid of the n best vertices i.e., $\bar{x} = \sum_{i=1}^{n} x_i/n$. if $f_1 \leq f_r < f_n$ accept the reflected point and terminate this iteration.

3. Expand

   If $f_r < f_1$ calculate the expansion point x_s from

$$x_s = \bar{x} + \xi(x_r - \bar{x})$$

   If f(x_s) ¡ f_r accept x_s and terminate the iteration; else if f(x_s) $\geq f_r$ accept x_r and terminate this iteration

4. Contract

   If $f_r > f_n$ perform a contraction. There are two types of contraction depending on the values of f_r,f_n,f_{n+1}. The outside contraction occurs when $f_n \leq f_r < f_{n+1}$ than

$$x_c = \bar{x} + \gamma(x_r - \bar{x})$$

   If f(x_c) $\leq f_r$ accept x_c, replace x_{n+1} terminate the iteration. else perform a

shrink step

The inside contraction occurs when $f_r \geq f_{n+1}$ than

$$x_c^{'} = \bar{x} - \gamma(\bar{x} - x_{n+1})$$

if f($x_c^{'}$)< f_{n+1} accept $x_c^{'}$ and terminate the iteration. Else perform a shrink step

5. Shrink

   Define a new set of vertices for the simplex

$$x_i^{new} = x_1 + \sigma(x_i - x_1)$$

The simplex method has two interesting properties 1. The Nelder-iteration requires one function evaluation if the iteration terminates in step 2, two function evaluations if the iteration terminates in steps 3 or 4 and n+2 evaluations if a shrink step occurs. The method requires fewer steps then comparable direct search method. 2. The next simplex is determined by the current simplex and the ordering.

In order to completely specify the optimization algorithms one needs a termination condition. For most problems,this condition is difficult to assess. This is also the case for inverse parameter estimation.

3.6.1 Experimental Data

Implicit in the inverse methodology is the need for experimental data. For multiphase flows, a number of quantities are typically measured including phase void fraction, ϵ, and pressure, P, across and inside the bed. [64] In the case of fluidized beds, void fraction measurements are conducted at prescribed points within the bed over fixed time intervals; thus the experimental $\epsilon_{s,f}$ is a time and distance averaged quantity. In lieu of actual experimental data, data is artificially generated using

$$\epsilon_i^{exp} = \epsilon_i^{calc} + \overline{\epsilon}\sigma \tag{3.34}$$

where ϵ_i^{calc} is the void fraction calculated by the direct solvers and $\overline{\epsilon}$ is the magnitude of pseudo-random noise added to ϵ_i^{calc}, and σ is a random number between -1 and 1.

This approach allows us to test the efficacy and stability of any given inverse procedure. It also allows us examine the effect of measurements uncertainty on inverse solution accuracy. Values of ϵ^{calc} in 3.34 were calculated using the following parameter values: A=0.63,B=4.14,C=1.28 and D=2.65. The fluidized bed used in the simulations below was based on a example in the MFIX distribution (apr. 1997 version). The fluidized bed is 2-d rectangular. It is 7cm wide by 100 cm high with 50 cm of bed and 50 cm of freeboard.

The bed portion is filled with solid spherical particles with d_p=400 and $\rho_p = 2000$. The MFIX input data file is included in Appendix C.

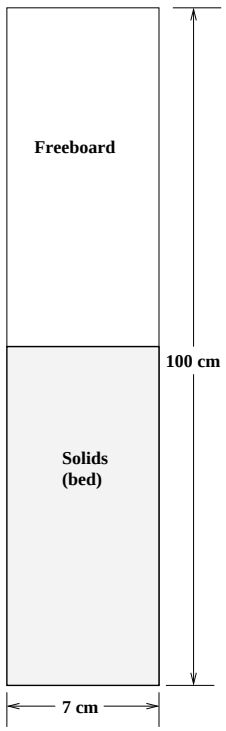

Figure 3.5: Schematic of fluidized bed used in simulations

3.7 The effect of initial guess on parameter estimation

In this section, we investigate two aspects of the inverse problem described. The first is the effect of the initial guess on the accuracy of the parameter estimation. The second is the effect of simulated probe placement used to gather experimental data

on parameter estimation. The second topic is an interesting and relatively new topic with a direct impact on the success of the inverse technique. In traditional inversion studies most of the research is focused on the mechanics of the inversion and how to increase the stability and speed of the process. Little attention is paid to how the "experimental data" used in the inversion is acquired. The exception to this rule being the so-called "big money inversion" (e.g. seismic,geophysical or atmospheric), where the cost of experiments can run into the millions).

The accuracy of an inverse solution for nonlinear problems, is strongly dependent on the quality of the initial guess. In this section, the effect of initial guess on inverse solution accuracy is considered. A number of computer experiments were performed in which various initial guesses, $P_o = (A_o, B_o, C_o, D_o)$, were used; generally the initially guesses were kept within $\pm 10\%$ of the known parameter values. In the first series of test only A and B were guessed,while C and D where set equal to their known values. The initial and final estimated values of A and B as well as the absolute relative error $E = abs[(\epsilon^{exp} - \epsilon^{calc})/\epsilon^{exp}]$ are shown in Tables 3.1 through 3.4 and Figures 3.6 through 3.8. Note that C and D were fixed during the minimization. And the experimental values where taken

percent error	A	B	C	D
0	0.043	0.126	0.0	0.0
5	0.206	0.101	0.0	0.0
10	0.202	0.036	0.0	0.0

Table 3.1: Abs. relative errors of initial guess A=.693,B=4.55,C=1.28,D=2.65

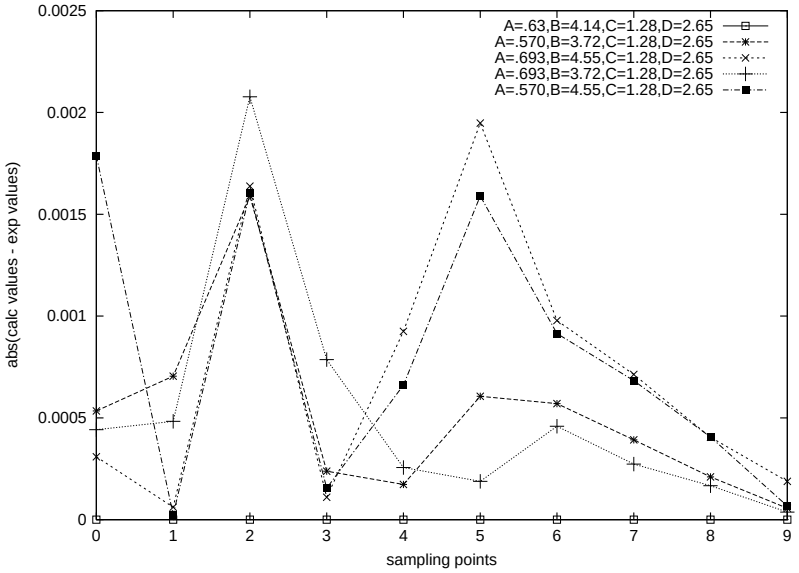

Figure 3.6: The effect of initial guess on convergence for data with 0 percent error

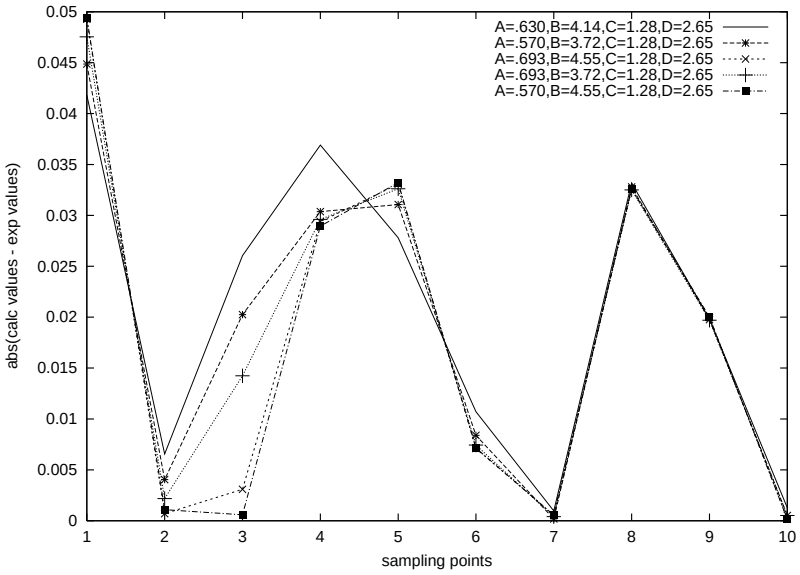

Figure 3.7: The effect of initial guess on convergence for data with 5 percent error

percent error	A	B	C	D
0	0.022	0.075	0.0	0.0
5	0.146	0.075	0.0	0.0
10	0.195	0.056	0.0	0.0

Table 3.2: Abs. relative errors of initial guess A=.693,B=3.72,C=1.28,D=2.65

percent error	A	B	C	D
0	0.029	0.111	0.0	0.0
5	0.211	0.183	0.0	0.0
10	0.206	0.130	0.0	0.0

Table 3.3: Abs. relative errors of initial guess A=.570,B=4.55,C=1.28,D=2.65

Figures 3.6 through 3.7 show the estimated solid void fraction, ϵ_s, at each of ten comparison points for a variety of initial guesses. In the case of noise-free measurements, the inverse algorithm converged quickly to the final parameter estimates, P_{final}. Estimated parameter values took on a fairly wide range of magnitudes: $0.603 \leq A_{final} \leq 0.644$ and $3.96 \leq B_{final} \leq 4.74$. An initial guess of $P_o = (.693, 3.72)$ produced the most accurate estimate; in this case the maximum error was less than 0.2 percent. However, the largest error in any case was on the order of 0.2 percent, well below the measurement error for most experiments. As more noise is added to the data, the accuracy of the inverse estimates decrease somewhat. However, figures 3.7 and 3.8 show that the effect of the initial guess on the final parameter estimate is small. From tables of results, it appears that the reconstruction remains stable with increasing experimental noise; the absolute relative error increases only slightly with additional noise, and in some instances actually decreases. From the final fraction data and parameters generated, it can be concluded that in the case where two

percent error	A	B	C	D
0	.008	0.043	0.0	0.0
5	.113	0.072	0.0	0.0
10	.206	0.065	0.0	0.0

Table 3.4: Abs. relative errors of initial guess A=.570,B=3.72,C=1.28,D=2.65

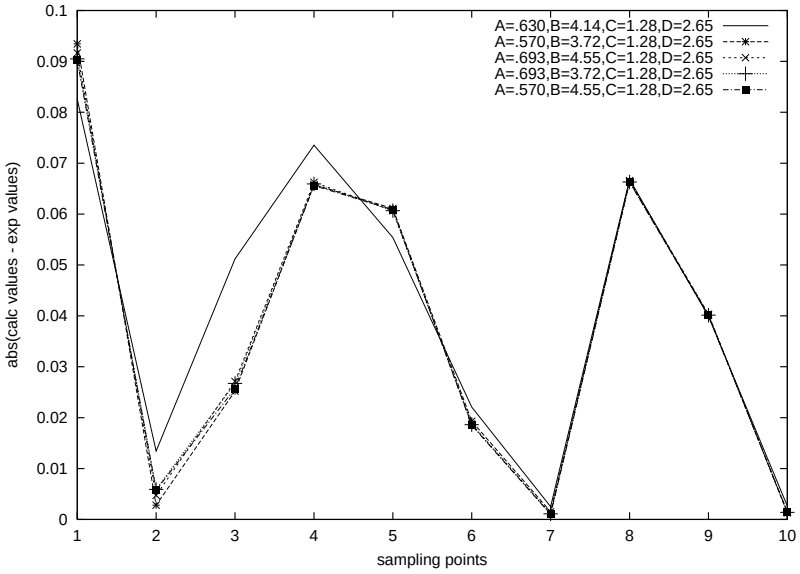

Figure 3.8: The effect of initial guess on convergence for data with 10 percent error

parameters are determined by the inverse procedure, remains relatively insensitive to the initial parameters chosen; moreover the inverse procedure produces results which are relatively accurate and that remain stable with increasing experimental error. The implications of the inverse procedure are clear. For fluidized bed systems the coupling of the solid and gas phases is a secondary effect. This would explain the success of many multiphase studies despite the lack of an adequate (or correct) interphase momentum term.

3.8 The effect of probe placement on reconstruction

Solutions to inverse problems require experimental data. Often the locations at which the experimental data are taken is determined by convenience rather than the potential information available at that those locations. The primary focus of this study is to find an optimal set of experimental points such that the inverse problem of interest converges more quickly and accurately. How to effectively sample spatial quantities in order to gain as much information about the process under investigation is a common problem in many areas including: hydrology, geology, geophysics,etc. The efficient sampling of spatial variables is just a small part of the much larger problem of proper experimental design. The focus of most spatial sampling studies have been the estimation of environmental data. Because, environmental data is often collected at a finite number of expensive monitoring stations, optimizing the sum total amount of information/data collected is extremely important. Environmental data collection provides a practical starting point for examining the feasibility of spatial sampling design in the the solution of inverse problems. The design of environmental data data collection networks is a subset of the more general problem of optimal experimental design. Optimal experimental design can be approached from two perspectives: the classical(frequentist) and the Bayesian (or informational). We believe the Bayesian approach to be superior to the classical approaches (for the

inverse systems under investigation) primarily because Bayesian approaches:

- Have been applied to experimental design for various physical processes (including environmental network design [45] [33] [16].
- Easily integrate a-prior information about the system of interest
- Are similar (in idea) to the "back of the envelope" approach used by most engineers.

An early discussion of the design of experiments from an information theoretic/Bayesian perspective was done by Lindley [24]. Lindley laid the foundation for the use of the Bayesian approach in experimental design by using the work of Shannon to determine a measure for amount of information gotten by performing an experiment. A number of researchers have generalized Lindley's work by showing it be equivalent to a decision problem [18] [9].

The use of information theory in inverse problems has been studied by a number of researchers [49] [68]. These researchers were interested in estimating the parameters of interest by direct application of Bayesian techniques. This differs from the approach taken here in which we use information theory to estimate the best measurement points, which are then used in a traditional inverse solution algorithm. A few researchers have taken this approach to the solution of the inverse problem. Emery and Nenarokomo used Fisher Information Matrix (FIM) approach to determine the optimal sensor (or probe) placement in order to estimate parameters for

a series of inverse heat transfer problems [1]. The FIM characterizes the sensitivity of the set of measurement to the unknown parameters. Emery and Nenorokomo use a d-optimal criteria or determinant criterion (max ln[det(FIM)]) to determine optimal probe placement within for inverse problems. This approaches suffers from the same problems that most techniques that use sensitivity analysis, most notably the calculation of the derivatives need to evaluate the sensitivity matrix.

In the next section, information theory is reviewed. In the sections that follow information theory's connection to experimental design is examined, an algorithm is developed which than applied to a two dimensional inverse heat conduction problem (IHCP). The IHCP problem seeks to determine the temperature (heat flux) from measured temperatures inside a heat conduction body. The IHCP is discussed in a number of references text [7] [2]. In the final sections, the techniques used to develop the IHCP experiment are applied to the problem of multiphase inversion.

3.8.1 Information and Entropy

In 1948, Claude Shannon [60] introduced a new way of thinking of information. Working in the context of a generalized communication system (see figure below) Shannon introduced two important ideas into the theory of information. The first idea is that information is a statistical concept, where the semantic meaning is of little importance to the design of an information theoretic system. The second idea derives from the first and implies that there is a unique function based on frequency distri-

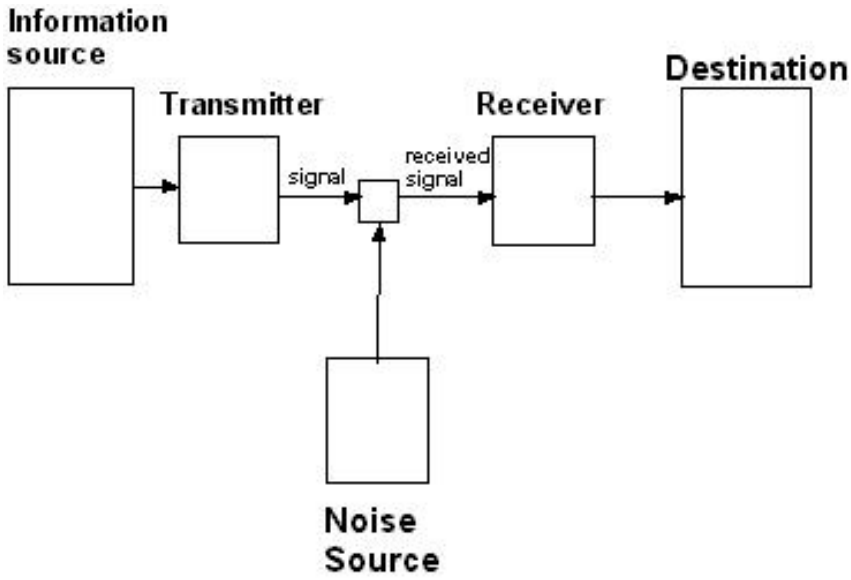

bution $p\{x_k\}$, that measures information. Information is a measure of uncertainty. Shannon's measure of information content (for a discrete frequency distribution) is shown below [58]: The average amount of information or Shannon entropy at the source X is

$$H(X) = -\sum_{k=1}^{n} p\{x_k\} ln(p\{x_k\}) \tag{3.35}$$

$p\{x_k\}$ where x_k stands for some proposition (for example the probability of transmitting a certain character in the communication system).

It is easy to see an analogy between Shannon's generalized communication system (figure 1) and the experimental measurements required to solve an inverse problem. We might think of an experiment as retrieving information from a complex source through a data (noisy) channel. The channel is described by a set of conditional prob-

abilities $p\{y_j|x_k\}$, which are the probabilities that some value x_k from the source will appear as some value,y_j at the sink (us). Thus, we might conclude that a maximally informative experiment is obtained when there is an equal chance of getting any value for the experimental data. By contrast as the range of experimental values narrow the uncertainty (or entropy) decreases.

Implicit, in the discussion above is the idea that what is being sent from the source to the receiver is error free (noise free). Because real-world systems are not error free, the idea of Shannon entropy needs to be extended. Transinformation or the system mutual information, I is a measure of the amount of information transferred between the sender and the receiver. In terms of the Shannon entropy

$$I = H(X) - H(X|Y) = H(Y) - H(Y|X) \tag{3.36}$$

where H(X) is the average information at the source (or transmitter). H(Y) is the average information at the receiver, H(Y|X) is the conditional average information of Y given the entropy of source (noise in the data channel). H(X|Y) is the condition average information of the source given the entropy of the sink. The transinformation is a change in the amount of information given some prior information about the source or the sink. Eq 3.36 is similar to Lindley's expression for the amount of

information obtained by doing an experiment,IE.

$$IE = \int E[H(\Theta) - H(\Theta|R)] \tag{3.37}$$

Here, $H(\Theta)$ is the entropy the parameter Θ before an experiment conducted. After the experiment is conducted and the results,R examined what the experimenter knows about Θ has changed,$H(\Theta|R)$ and is dependent on what was observed. If Θ and R are independent, that is knowing R does change the distribution of Θ , IE = 0. Analogously, when the sending source and receiver are independent, the transinformation is also zero. In the case of a noise free channel, H(X|Y) = H(Y|X) = 0 and I = H(X) = H(Y). In the case of additive noise, with probability discrete density function, ϕ_k

$$I = H(Y) + \sum_{k=1}^{n} \phi_k(log\phi_k) \tag{3.38}$$

In the next section, we explore the connection between the spatial structure of an experiment and the amount of information that can be divined from it.

Connections

In this section we connect information theory and the selection of optimal experimental points in inverse problems. As described above, the inverse heat problem under investigation seeks to estimate the temperature at a few points on the boundary of the physical domain by temperature measurements made in its interior. Using

information theory, we hypothesize that the more spatially uncorrelated the experimental temperature measurements, the less uncertainty or entropy we can expect from each additional measurement point. For example, in the extreme case where all measurements are made at a single point (or very close to one another), each measurement after the initial one provides no additional information or surprise. Thus, we might conclude that by minimizing the correlation between points we will be able to produce a set of measurement points that will improve the efficiency of the inverse procedure by increasing the information content of the measurement. In order to explore this hypothesis in more detail let us assume a form for the experimental data. A common assumption is that experimental data can be modeled by a two dimensional Gaussian field,p.

$$p(\mathbf{T}|\mu, \mathrm{C_{ij}}) = ((2\pi)|\mathrm{C_{ij}}|)^{-1/2}\exp[\frac{1}{2}(\mathbf{T}-\mu)^{\mathrm{T}}\mathrm{C_{ij}^{-1}}(\mathbf{T}-\mu)] \tag{3.39}$$

p is the probability of a temperature T appearing at grid point (i,j). $|C_{ij}|$ is the determinate of a covariance matrix. The covariance matrix, C_{ij} is generated from a covariance function, which provides a measure of the spatial structure between point i and j. If we assume a noise free data channel, and substitute equation 3 into equation 2 then we find that

$$I = H(X) = ln\sqrt{2\pi}|C_{ij}| \tag{3.40}$$

The entropy at the receiver, H(X) increases with the determinant of the spatial

covariance. Thus, the problem of the maximizing the information content of a experiments becomes isomorphic to maximizing, $ln|C_{ij}|$ or in the one-dimensional the problem reduces to maximizing the log of the variance. The maximization of $ln|C_{ij}|$ is known as a Bayes D-optimal design criteria for experimental design. .

In information theory terms, the maximum value of I is called the capacity, thus we might conclude the most information rich data points are the ones that maximize the transinformation or the ones that produce the capacity. On the surface, the arguments above are sound and lead to a seemly logical design criteria. The best measurement locations are points that make the probability of any experimental values equally likely.

However, on closer examination, we are missing one vital aspect of experimental design – the incorporation of prior information/experience into the design. For example, in an inverse problem we might assume the measurements points in the interior are more or less informative then those on the boundary. Incorporating priori information into experimental design is at the heart of Bayesian approaches.

Currently, the only way to incorporate information into the experimental design is through the covariance function (see section 3.3). The covariance function allows us to manipulate the spatial relationship between between physical points, but not the values (or relative values) at measurement locations. In essence, information is added to the system via manipulation of a probability density function. In order to add additional information to the system, we propose to augment the elements of

covariance matrix with weighting factors.

If we assume a noisy data channel with a Gaussian noise structure E_{ij}, the equation above is little changed

$$I = \frac{1}{2} ln \left(1 + \left(\frac{|C_{ij}|^2}{|E_{ij}|^2} \right) \right) \tag{3.41}$$

The expression $\frac{|C_{ij}|^2}{|E_{ij}|^2}$ is ratio of signal to noise.

If the structure of the noise is constant then the transinformation and capacity are only a functions of the covariance and thus we conclude the location of the experimental measurements are invariant with respect to error. If however, there is prior information about the spatial structure of the system error, that information should be incorporated into the experiment through the weighted covariance function.

The covariance function

As stated above, the spatial covariance function covar(ij), provides a measure of the correlation structure between points i and j. The common forms of the covariance function decay as a function of distance between the two points. A common covariance function for isotropic processes is

$$covar(ij) = exp^{-\alpha d_{i,j}} \tag{3.42}$$

Where $d_{i,j}$ is the distance between points i and j located at points (x_i,y_i) and (x_j,y_j) respectively, and α is the cutoff (interaction) parameter which is selected based on

the physical processes being modeled. As α increases, covar(ij) steepens, implying that the two points must be closer together in order for their values to be correlated. Often α is chosen based on a process characteristic length scale and the geometry of the problem.

A different covariance function is the Bessel type function:

$$covar(ij) = bd_{i,j}K(bd_{i,j}) \tag{3.43}$$

Both functions (3.42 and 3.43) have been used extensive in design of environmental data collection networks [12]. Note that both covariance functions are stationary or only a function of the distance between between points (not the position of the data points) and symmetric, that is covar(ij) = covar(ji). The environmental monitoring The covariance matrix is generated from the covariance function by

$$\sum_{i}^{n}\left[\sum_{j\neq i}^{n}[C_{ij} = covar(ij)]\right] \tag{3.44}$$

Where n is the total number of sampling points or measurement points. Because the covariance function is central to the arguments that follow, a simple example is presented in order to clarify the definitions. Given a domain with 3 sampling point (n=3) A,B,C at locations (1,1),(1,5),(4,5) respectively, and using the exponential covariance functions with $\alpha = .1$.

$$C = \begin{bmatrix} 1.000 & 0.201 & 0.082 \\ 0.201 & 1.000 & 0.407 \\ 0.082 & 0.407 & 1.000 \end{bmatrix} \tag{3.45}$$

This example illustrates a number of things about the covariance matrix. Firstly, the matrix is symmetrical, which is not surprising given the function used to generate it. Secondly, the eigenvalues of C will always be real. Finally, the maximum value of the determinant (or natural log of the determinant) is achieved with an identity matrix. Which occurs when there is a sufficient separation (either because alpha is sufficiently large or the distance between the points is great) between points. This jives nicely with our original hypothesis that maximum entropy is achieved when there is no correlation between points. However, many points may satisfy this criteria, so it is necessary to add other criteria.

In order to use ideas above for inverse problem, some modification need to be made in order to account for additional information. In the results to follow, apriori information about the processes under study, was incorporated into an optimal spatial sampling algorithms through the use of a measurement point weighting factor. The weighting factor acknowledges the fact that even under ideal conditions not all measurement points are equal. With the inclusion of the weighting factor, the covariance function is

$$covar^*(i,j) = w(i,j)covar(i,j) \tag{3.46}$$

This new covariance function is now non-stationary but defined in terms of a stationary covariance function.

For example in the inverse problem under investigation, we might speculate that the points closest to the boundary have less "information", since we know (at least partially) the boundary condition, then points in the interior the domain. The introduction requires little modification to existing theory. The covariance matrix is:

$$\sum_{i}^{n}\left[\sum_{j\neq i}^{n}[C_{ij} = w(i,j)covar(i,j)]\right] \tag{3.47}$$

Where n is the total number of sampling points and w(i,j) is the weighting factor.

3.8.2 Numerical algorithm

Using the ideas above, an algorithm was designed to find the information theoretic optimal sampling location for the inverse problem. A number of assumptions where used in the design of the algorithms including: the experimental data can be modeled by a random Gaussian field, the number of locations is constant, the relationship between measurement location can be modeled by a stationary covariance functions, apriori information is included into the objective function (eg. a weighting function)

1. Set alpha for the covariance function.

2. Select the number of measurement points,mp.

3. Determine the relative value of the spatial information for the experiment (not all measurement location are created equal). This is where the inverse problem may differ slightly from the standard maximum entropy sampling problem. For processes that can be modeled by elliptical and parabolic partial differential equations, the boundaries of the object are known (to some degree) and thus may provide less "information" about the process. As we move into the interior of the object, we are less certain about the information. This type of apriori information can incorporated through the use of a weighting factor for the covariance function. When all the points are believed have an equal amount of uncertainty the weighting factor is not used. $w(ij) = 1$.

4. Select locations of the potential measurement points,mp. For convenience, measurement locations are limited to grid points (on the computational grid).

5. Calculate the covariance matrix,C_{ij} from the covariance function and weighting factor.

6. Calculate ObjFunc = $\ln(\det(C_{ij})$.

7. if ObjFunc is a maximum stop calculation else return to step 4.

The problem of finding the optimal points is reduced to an unconstrained optimization problem. In the current study, genetic algorithms were used to solve this optimization.

Once the "optimal points" are determined they are used in the inverse procedure to find the parameter vector.

3.8.3 The number of measurement of points

The heart of the inverse procedure is the evaluation of the objective function and the selection of the next parameter to test in the forward problem. The evaluation of the objective is function is done at several measurement points,np.

$$d_{residual} = \sum_{i}^{np} objFunc(i) \tag{3.48}$$

As stated previously, the purpose of this study is find a set of measurement points which provide us with the maximum amount of information about the process under study, implicit in the discussion so far, is that the number of measurement points is fixed and selected beforehand. The number of measurement points plays a key role in the effectiveness of the inverse procedure. As we might expect, as the number of measurement points increase the the marginal utility of each point decreases. In addition, the number of points strongly influences the relationship between the $d_{residual}$ and the parameters selected by the optimization algorithms. If there is no relationship between the parameters selected by the optimization and the objective used to produce the next set of parameters the results can be disastrous.

3.8.4 Application of the algorithm to IHCP

Results without the weighting factor

In this section, we use the algorithms above without a weighting factor to determine the optimal measurements points. Assume the following conditions for the inverse problem described above: the domain is 9in by 9in, $\alpha = .5$, the number of measurement location is four, and each point has an equal weighting factors of 1 (eg. $w_{ij} = 1$). Using the algorithm above, the "optimal" measurement locations were calculated to be the corners of the domain mp=(0.0,0.0),(0.0,9.0),(9.0,0.0),(9.0,9.0). The optimal locations should come as no surprise given the previously presented ideas As we increase the value of alpha, the covariance function steepens, implying interactions between measurements are more short-ranged. Viewed in these terms the covariance function is merely the overlap of "spheres of influence". The less the overlap, the larger the covariance. Using these measurement points the inverse method generates the the following parameter set, p_{inv}=(9.46,6.01,9.78,9.06) which compare poorly with parameter vector p_{true} =(7.0,7.5,9.0,10.0) used to generate the experimental "data".

Results with weighting factor

Most experimentalist (and even some theorist) have prior information about the inverse (or physical) processes they are studying. For example in the current problem, we have some knowledge of the relative value of the spatial information. As we speculated earlier, we are more certain about the temperatures near the object

boundary than temperatures in the interior of the object. Thus, a reasonable point weighting factor (pwf) might be one in which we linearly interpolate between zero uncertainty (pwf$(x_i, y_i) = 0$) at the boundary to a maximum uncertainty (pwf(x_i, y_i) $= 1$) of in the center of the domain. For the current problem, the pwf for each grid point was generated using Poisson's' equations in a technique similar to one used in algebraic grid generation.

In order to be used with the covariance function, the weighing factor must be an "average" of the point weighting factor. For the current study

$$w_{ij} = 1/2(pwf(x_i, y_i) + pwf(x_j, y_j) \tag{3.49}$$

The table below shows the results of the inverse procedure with various "optimal measurement" points.

$$C = \begin{bmatrix} np & \alpha & p_{inv} \\ 4 & -1.50 & 9.29, 6.33, 9.04, 9.95 \\ 4 & -0.05 & 8.94, 7.27, 8.36, 10.04 \\ 4 & -0.50 & 9.29, 6.33, 9.04, 9.98 \end{bmatrix} \tag{3.50}$$

Though not perfect, the results above show how a naive implementation of the experimental design ideas presented above, can effectively increase the amount of information that is available for an inverse technique "to process" during a simple

IHCP.

3.8.5 Application to multiphase inversion

In the previous section we applied the theory of design to an inverse heat conduction problem. We saw that by clever application of information theory we are able to increase the speed of convergence for the inverse procedure. In this section, we will apply these same inverse and experimental design techniques to the multiphase inversion. In fluidized bed experiments, the most commonly measured variable is the air or particle voidage fraction, ϵ_f or ϵ_p. Using, the techniques above, the fluidized bed is run with three different measurement configurations: clustered measurements, random measurements and evenly distributed measurements. We will use the same

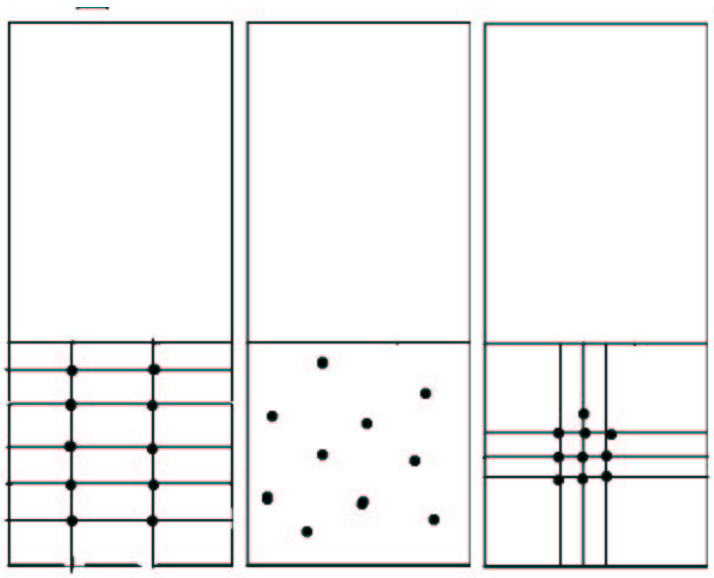

Figure 3.9: Measurement configuration for multiphase flows even,random and clustered configurations

covariance equation used in the previous example. The physical features of the fluidized bed are given above. The covariance matrix for the clustered measurements is:

$$C_{clus} = \begin{bmatrix} 1.0 & 0.85 & 0.85 \\ 0.85 & 1.0 & 0.85 \\ 0.85 & 0.85 & 1.000 \end{bmatrix} \tag{3.51}$$

det[C] = .060750 The random measurement covariance matrix is:

$$C_{rand} = \begin{bmatrix} 1.0 & 0.45 & 0.28 \\ 0.45 & 1.0 & 0.73 \\ 0.28 & 0.73 & 1.0 \end{bmatrix} \tag{3.52}$$

det[C] = .37

The even configuration

$$C_{rand} = \begin{bmatrix} 1.0 & 0.15 & 0.15 \\ 0.15 & 1.0 & 0.15 \\ 0.15 & 0.15 & 1.0 \end{bmatrix} \tag{3.53}$$

det[C] = .94

Using the weighting scheme (interior points have a higher weight than boundary points) and arguments above, we would expect that the "even" configuration to have the highest entropy (and hence information content). The results of the simulation

show this to be true.

percent error	A	B
0	.009	0.063
5	.19	0.09
10	.30	0.10

Table 3.5: Abs. relative errors of initial guess A=.570,B=3.72 for clustered configuration

percent error	A	B
0	.007	0.045
5	.12	0.08
10	.14	0.07

Table 3.6: Abs. relative errors of initial guess A=.570,B=3.72 for random configuration

percent error	A	B
0	.007	0.021
5	.08	0.07
10	.10	0.08

Table 3.7: Abs. relative errors of initial guess A=.570,B=3.72 for even configuration

From the three tables above, we see that the absolute relative error improves with the high information (even) configuration. Based on what was observed with the IHCP (and commonsense), it appears that at least for inverse parameter estimation in multiphase flows – careful selection of the measurement points can have an impact on the success of the inverse technique.

In this section we have reviewed the basics of the continuum multiphase equations and proposed a interesting and novel inverse technique to estimate the momentum exchange terms. In addition, we examined the issue of selecting the proper measurement

location required by the inversion. We developed an information theory approach to experimental design and applied these results to a prototype inversion (e.g. inverse heat conduction) and than expanded the approach to the full multiphase inversion. The result in both cases was that as the information content of the measurement location increased (as defined by the covariance matrix and the transinformation) the inverse procedure produced better and faster results.

Chapter 4

Conclusion

In this study we examined two topics: the use of lagrangian methods on dense phase flows and the application of inverse methods to study gas-solid flows. Though seemly disparate topics they are infact connected. Both topics are attempts to understand how momentum is transferred between phases in multiphase flows. To review:

- Lagrangian methods use an explicit coupling of the two phases. That is the momentum transfer is a natural result of the technique. The main assumption used in this type of modeling is the nature of collision between particle (if the flows are a sufficiently high mass loading).

- The continnum methods used in the inverse problem attack the problem of momentum coupling in a different manor. Continuum methods seek to extend the well understood Navier-Stokes equations by additional particle momentum and continuity equations.

In reviewing the results presented in the previous section we can can conclude several interesting things. Some of which are self-evident other not so.

- Euler-Lagrangian methods are now a viable alternative to multiphase continuum methods in dense phase (e.g. high mass loaded) solid-gas flows.

- The main assumptions in the Euler-Lagrangian method is the type and form of the collision between particles and at low Stokes numbers the form of the particle dispersion function.

- The Lagrangian simulation performed for this study (see Chapter 2) captured a number previously uncaptured features of dense solid-gas phase flows including: The gas phase velocity profile skew present in dense systems. More work (analytic and computational) needs to be done to understand the flow physics involved. The entrapment of small particles in a turbulent boundary layers.

- Two phase continuum methods rely a variety (often bad) assumption about the type and nature of the momentum exchange between phases. They often use empirical or semi-empirical forms to close the equation set.

- In this study we examined the feasibility of inverse methods to parameter estimation in multiphase flows. We found that inverse methods provide an excellent mechanism to "tune" computational results to experimental data.

- By using an information theory based experimental design we are able to increase the accurate and speed of convergence of the inverse methodology.

Bibliography

[1] A.V. Nenarokomov A.F. Emery and T.D. Fadale. Uncertainties in parameter estimation: the optimal experiment design. *International Journal of Heat and Mass Transfer*, 43:3331–3339, 2001.

[2] O. Alifanov. *Inverse Heat Transfer Problems*. Springer-Verlag, Berlin, 1994.

[3] M.P. Allen and D.J. Tildesley. *Computer Simulation of Liquids*. Oxford University Press, Oxford,UK, 1989.

[4] H. Arastoopour, C.-H Wang, and S.A. Weil. Particle-particle interaction force in a dilute gas-solid system. *Chemical Engineering Science*, 37:1379–1384, 1982.

[5] T. R. Auton and and M. Prud'Homme J.C.R.Hunt. The force exerted on a body in inviscid unsteady non-uniform rotational flow. *Journal of Fluid Mechanics*, 197:241–257, 1988.

[6] J. Bardina, J.H. Ferziger, and W.C. Reynolds. Improved subgrid models for large eddy simulation. *AIAA paper*, 80:1357, 1980.

[7] J.V. Beck, B. Blackwell, and S.R. Clair. *Inverse Heat Conduction.* John Wiley and Sons, New York, 1985.

[8] A. Berlemont, P. Desjonqueres, and G. Gousebet. Particle lagrangian simulation in turbulent flow. *International Journal of Multiphase Flow*, 16:19–34, 1990.

[9] J.M. Bernardo. Expected information as expected utility. *Annals of Statistics*, 7:686–690, 1979.

[10] T. Bonner and F. Durst. Dispersed two-phase flow: Its experimental investigation and numerical prediction. *Modelling and Solution Techniques for Multiphase Flow*, 3:53–113, 1985.

[11] E.J. Boyle, W.N. Sams, M. Syamlanl, and S.M. Cho. Mfix validation studies–dec. 1994 to nov. 1995. Technical Report DOE/METC–97/1042:, Morgantown Energy Technology Center, Morgantown Energy Technology Center, WV (United States), 1998.

[12] R.L. Bras and I. Rodriguez-Iturbe. *Random Function and Hydrology.* Dover Publications, New York,New York, 1993.

[13] R.P. Brent. *Algorithms for minimization without derivatives.* Prentice-Hall, Englewood Cliffs, NJ, 1973.

[14] R. S. Brodkey. *The Phenomena of Fluid Motions.* Dover Publications, New York, 1995.

[15] R.P.Gilbert L. Zhongyan J.L. Buchanan. Direct and inverse problems in ocean acoustics. *Nonlinear analysis*, 30:1535, 1997.

[16] W. Caselton and J. Zidek. Optimal monitoring network designs. *Statistics and Probability Letters*, 2:223–227, 1984.

[17] C.Crowe, M.Sommerfeld, and Y. Tsuji. *Mulitphase Flows with droplets and particles*. CRC press, Boca Raton,Florida, 1998.

[18] K. Chaloner and I. Verdinelli. Bayesian experimental design. *Statistical Science*, 10:273–304, 1995.

[19] C.T. Crowe, M.P. Sharma, and D.E. Stock. The particle-source-in-cell methods for gas droplet flow. *Journal of Fluid Engineering*, 99:325, 1997.

[20] C.T. Crowe, T.R. Troutt, and J.N. Chung. Numerical models for two-phase turbulent flows. *Annual Review of Fluid Mechanics*, 28:11–43, 1996.

[21] D.Burry and G.Bergeles. Dispersion of particles in anisotropic turbulent flows. *International Journal of Multiphase Flow*, 16:651–664, 1990.

[22] D. A. Drew and R. T. Lahey. Numerical simulation of inelastic, frictional particle-particle interaction. *Particulate two-phase flow, M. Roco (Ed.)*, pages 509–566, 1993.

[23] P. DuChateau. An inverse problem for the hydraulic properties of porous media. *SIAM Journal of Math. Anal*, 28:611–632, 1997.

[24] D.V.Lindley. On the measure of information provided by an experiment. *Ann. Math. Stat*, 27:986–1005, 1956.

[25] J.K. Eaton and J.R. Fessler. Preferential concentration of particles by turbulence. *International Journal of Multiphase Flow*, 20,Supplement:169–209, 1994.

[26] G. Hetsroni Editor. *Handbook of multiphase systems.* Hemisphere Pub. Corp – McGraw-Hill, New York, 1982.

[27] S. Elghobashi and G. C. Truesdell. On the 2-way interaction between homogeneous turbulence, turbulence and dispersed solid particles 1. turbulence modification. *Physics of Fluids*, 5:1790–1801, 1993.

[28] H. Enwald, E. Peirano, and A.E. Almstedt. Eulerian two-phase flow theory applied to fluidization. *International Journal of Multiphase Flow*, 22:21–66, 1997.

[29] J.H. Ferziger and M. Peric. *Computational Methods for Fluid Dynamics.* Springer-Verlag, Berlin, 1996.

[30] A. Gavrus, E. Massoni, and J.L Chenot. The rheological parameter identification formulated as an inverse finite element problem. *Inverse Problems in Engineering*, 7:1–41, 1999.

[31] D. Gidaspow. *Multiphase Flow and Fluidization: Continuum and Kinetic Theory Description.* Academic Press, NY, 1994.

[32] D.E. Goldberg. *Genetic algorithms in search, optimization, and machine learning.* Addison-Wesley, New York,New York, 1989.

[33] P. Guttorp, N. Le, and P. Sampson. Using entropy in the redesign of environmental monitoring network, 1993.

[34] R.W. Hamming. *Coding and Information Theory.* Prentice-Hall, Englewood Cliffs, NJ, 1980.

[35] G. Hestroni. Particle-turbulence interaction. *International Journal of Multiphase Flow*, 15:735–746, 1989.

[36] G. Bruckner S.Handrock-Meyer H.Langmach. An inverse problem from 2d ground-water modelling. *Inverse problems*, 14:835, 1998.

[37] M. Ishii. *Thermo-fluid Dynamic Theory of Two-Phase Flow.* Eyrolles, Paris, 1975.

[38] Tsong-Hai Jean and J. Peddison. Mathematical modeling of particulate suspension flows in vertical circular pipes. *International Journal of Engineering Science*, 39:1167–1189, 200.

[39] S.L. Lee and F. Durst. On the motion of particles in turbulent duct flows. *International Journal of Multiphase Flow*, 8:125, 1982.

[40] K.S. Lim, J.X. Zhu, and J.R. Grace. Hydrodynamics of gas-solid fluidization. *International Journal of Multiphase Flow*, 21. Suppl:141–193, 1995.

[41] E. Loth. Numerical approaches for motion of dispersed particles, droplet and bubbles. *Progress in Energy and Combustion Science*, 26:161–223, 2000.

[42] C.K.K. Lun and H.S. Liu. Numerical simulation of dilute turbulent gas-solid flows in horizontal channels. *International Journal of Multiphase Flow*, 23:575–605, 1997.

[43] R.W. Lyczkowski, D. Gidaspow, C.W. Solbrig, and E.D. Hughes. Characteristicsand stability analyses of transient one-dimensional two-phase flow equationsand their finite difference approximations. *Nuclear Science and Engineering*, 66:378396, 1978.

[44] M. Maxey and J. Riley. Equation of motion for a small rigid sphere in a nonuniform flow. *Physics of Fluids*, 24:883–889, 1983.

[45] F.J. Alonso M.C. Buesco, J.M. Angulo. A state-space model approach to optimum spatial sampling design based on entropy. *Environmental and Ecological Statistics*, 5:29–44, 1998.

[46] J.B. McLaughlin. Numerical computation of particles-turbulence interaction. *International Journal of Multiphase Flow*, 20,Suppl:211–232, 1997.

[47] M.H.Wright. Direct search methods: once scorned,now respectable. In D.F. Griffiths and G.A. Watson, editors, *Numerical Analysis 1995(Proceedings of the*

1995 Dundee Biennial Conference in Numerical Analysis), pages 191–208. Addison Wesley Longman, 1996.

[48] D. Migdal and D.V. Agosta. A source flow model for continuum gas-particle flow. *ASME J. Applied Mechanics*, 34E:860, 1967.

[49] Ali Mohammad-Djafari. A full bayesian approach for inverse problems. 2:223–227, 1984.

[50] S.A. Morsi and A.J. Alexander. A investigation of particle trajectories in two phase flow systems. *Journal of Fluid Mechanics*, 55:193–208, 1972.

[51] J.A. Nelder and R. Mead. A simplex method for function minimization. *Computer Journal*, 7:308–313, 1965.

[52] M. Syamlal W. Rogers T.J. O'Brien. Mfix documentation theory guide. Technical Report DOE/METC–94/1004, Morgantown Energy Technology Center, Morgantown Energy Technology Center, WV (United States), December 1993.

[53] M. Syamlal W. Rogers T.J. O'Brien. Mfix documentation user's manual. Technical Report DOE-METC–941013, Morgantown Energy Technology Center, Morgantown Energy Technology Center, WV (United States), December 1993.

[54] M.N. Ozisik. *Heat Conduction.* John Wiley and Sons, New York, 1993.

[55] M. Rudnicki P. Neittaanmaki and A. Savani. *Inverse Problems in Optimal Design in Electricity and Magnetism.* Oxford University Press, Oxford,UK, 1996.

[56] W.H Press, S.A. Teukolsky, W.T Vetterling, and B.P.Flannery. *Numerical recipes in C: the art of scientific programming.* Cambridge University Press, Cambridge, 1992.

[57] J.N. Reddy. *An introduction to the finite element method.* McGraw-Hill, New York, 1993.

[58] F.M. Reza. *An Introduction to Information Theory.* Dover Publications, New York,New York, 1994.

[59] S. Schwarzer. Sedimentation and flow through porous media: Simulating year dynamically coupled discrete and contiuum phases. *Physical Review. E*, 52:6461, 1995.

[60] C. Shannon. A mathematical theory of communication. *The Bell System Technical Report*, 27:379–423, 1948.

[61] J.S. Shirolkar, C.F.M. Coimbra, and M.Q. McQuay. Fundamental aspects of modeling turbulent particle dispersion in dilute flows. *Progress In Energy and Combustion Science*, 22:363–399, 1996.

[62] S.L. Soo. *Multiphase Fluid Dynamics.* Science Press, Beijing,China, 1990.

[63] D.B. Spalding. Numerical computation of multi-phase fluid flow and heat transfer. In C.Taylor, editor, *Recent Advances in Numerical Methods in Fluids.* Pineridge Press, 1980.

[64] J.S. Harlow G.E. Fashching P. Nicoletti J.L. Spenik. Observations of a fluidized bed using capacitance imaging. *Chemical Engineering Science*, 48:642–659, 1993.

[65] M.G. Srinivasan and E.D. Doss. Momentum transfer due to particle-particle interaction in dilute gas-solid flows. *Chemical Engineering Science*, 40:1791–1792, 1985.

[66] P.L Stoffa and M.K. Sen. Nonlinear multiparameter optimization using genetic algorithms in plane wave seismograms. *Geophysics*, 56:1794–1810, 1991.

[67] S.V.Pantakar. *Numerical Heat Transfer and Fluid Flow.* McGraw-Hill, 1980.

[68] A. Tarantola. *Inverse Problem Theory.* Elsevier Science Publishers B. V., Amsterdam, The Netherlands, 1986.

[69] S. Timoshenko. *Theory of elasticity.* McGraw-Hill, New York, 1951.

[70] Y. Tsuji and Y. Morikawa. Ldv measurements of an air-solid two-phase flow in a horizontal pipe. *Journal of Fluid Mechanics*, 120:385–409, 1982.

[71] Y. Tsuji, Y. Morikawa, and H. Shiomi. Ldv measurements of an air-sold two phase flow in a vertical pipe. *Journal of Fluid Mechanics*, 139:417–434, 1984.

[72] O.R. Walton. Numerical simulation of inelastic, frictional particle-particle interaction. *Particulate two-phase flow, M. Roco (Ed.)*, pages 884–920, 1993.

[73] T.H. Wood and S.M. Grace. Inverse aeroacoustic problem for a rectangular wing. *AIAA journal*, 38:203, 2000.

[74] J. Young and T. Hanratty. Optical studies of turbulent motion of solid particles in a pipe flow. *Journal of Fluid Mechanics*, 231:665–688, 1991.

Appendix A

Tsuji data

A.1 Raw Tsuji Data

The data in this section was given to the author of this report by Professor Yutaka Tsuji of Osaka University. Most of the data is from the Tsuji paper [71].

A.1.1 Data for Figure 5

```
mu=3.4;uc=10.7
2r/D    .933    .800    .667    .533    .400    .267    .133    0
        .808    .932    1.008   1.040   1.032   1.012   1.006   1.0

mu=2.9;uc=11.4
2r/D    .933    .800    .667    .533    .400    .267    .133    0
        .804    .924    .990    1.026   1.036   1.026   1.010   1.0

mu=2.6;uc=11.9
2r/D    .933    .800    .667    .533    .400    .267    .133    0
        .770    .896    .964    1.004   1.018   1.020   1.010   1.0

mu=2.1;uc=12.1
2r/D    .933    .800    .667    .533    .400    .267    .133    0
        .732    .860    .932    .972    .996    1.0     1.00    1.00

mu=1.3;uc=13.1
2r/D    .933    .800    .667    .533    .400    .267    .133    0
        .744    .840    ,904    .952    .982    .996    .998    1.0

mu=.7;uc=12.2
2r/D    .933    .800    .667    .533    .400    .267    .133    0
        .682    .784    .860    .908    .944    .976    .992    1.0

mu=0.0;uc=13.4
2r/D    .933    .800    .667    .533    .400    .267    .133    0
        .672    .774    .840    ,890    .932    ,964    .998    1.0
```

A.1.2 Figure 6 data

```
mu=3.2;uc=10.8
```

2r/D	.933	.800	.667	.533	.400	.267	.133	0
	.815	.932	.990	.996	1.004	1.010	1.008	1.0

mu=1.9;uc=11.9

2r/D	.933	.800	.667	.533	.400	.267	.133	0
	.731	.846	.912	.960	.988	.997	.999	1.0

mu=1.3;uc=12.8

2r/D	.933	.800	.667	.533	.400	.267	.133	0
	.702	.840	.870	.912	.950	.980	.992	1.0

mu=.5;uc=13.1

2r/D	.933	.800	.667	.533	.400	.267	.133	0
	.690	.783	.846	.900	.932	.970	.986	1.0

mu=0.0;uc=13.4

2r/D	.933	.800	.667	.533	.400	.267	.133	0
	.670	.772	.840	.896	.928	.960	.983	1.0

A.1.3 Figure 7 data

mu=3.0;um=15.3;uc=19.5

2r/D	.933	.800	.667	.533	.400	.267	.133	0
	.349	.350	.375	.410	.430	.450	.450	.449

mu=2.2 um=15.4;uc=19.5

2r/D	.933	.800	.667	.533	.400	.267	.133	0
	.299	.309	.328	.355	.400	.430	.458	.430

mu=1.2;um=16.0;uc=20.0

2r/D	.933	.800	.667	.533	.400	.267	.133	0
	.240	.299	.313	.332	.356	.380	.423	.407

A.1.4 Figure 8 data

u=3.6;um=7.89;uc=8.07

2r/D	.933	.800	.667	.533	.400	.267	.133	0
	.698	.713	.753	.756	.751	.751	.750	.757

```
mu=2.0;um=8.00;uc=8.00
2r/D    .933    .800    .667    .533    .400    .267    .133    0
        .595    .620    .645    .675    .681    .690    .691    .70

mu=1.1;um=7.96;uc=9.65
2r/D    .933    .800    .667    .533    .400    .267    .133    0
        .565    .577    .595    .615    .615    .625    .639    .639
```

A.1.5 Figure 9 data

```
2r/D    .933    .800    .667    .533    .400    .267    .133    0
        .795    .860    .897    .925    .935    .947    .955    .958

2r/D    .933    .800    .667    .533    .400    .267    .133    0
        .745    .810    .855    .885    .905    .924    .925    .925

2r/D    .933    .800    .667    .533    .400    .267    .133    0
        .745    .800    .830    .865    .890    .905    .922    .925
```